# Chapter 7 Multifunctional silver contained bioactive glass-ceramic scaffold for bone tissue engineering

## 7.1 Introduction

A recent trend in materials design and production is to produce materials with multi characteristics like multi-elements, multi-structures, multi-functions, fast recovery, biocompatibility, etc. Furthermore, a major challenge is posed for regeneration of large size bone defects generally caused due to infections, trauma, accidents, tumors or genetic malformations in the human body. Scaffolds with porous structure are exhibiting high potential for bone tissue engineering and their interconnected network structure facilitates sufficient space for cell migration and ingrowth of new bone as well as soft tissues [73,158,159]. Yan et al. have prepared highly ordered mesoporous bioactive glasses and demonstrated higher bioactivity than the sol-gel derived bioactive glasses [76]. The porous bioactive glass scaffolds demonstrate a controlled rate of surface reactions and biodegradation and hence the bioactivity would be achieved much faster [160]. The bioactive scaffolds are showing foremost progress in bone tissue engineering, which are due to their significant growth factors, gene and drug deliveries [161]. It was highlighted that an ideal scaffold for bone tissue engineering should have high bioactivity, excellent osteoconductivity, good biodegradability, ability to deliver cells, appropriate mechanical properties, porous structure and ease of fabrication for commercial purposes [162]. Porosity of the scaffold plays an important role and it must be interconnected porous network with a wide variety of pore sizes like macropores (>400–500 μm) which allow tissue ingrowth and vascularization and the microporous pores (2-50nm) promote protein adhesion and consequently cell attachment and growth [100][77]. Furthermore, the scaffolds should be fabricated with bioactive materials for better interaction with hard and soft tissues

and thus it enhances the fast recovery of the patients. Porous matrixes have been fabricated by various methods like polymer-sponge method, surfactant foaming, polyethylene glycol (PEG) particulates, polyethylene (PE) powders and freezing of camphene-based suspensions etc. [100,163–166]. Importantly, the pore size and porosity need to be controlled, since the porous structure permits the early migration of new bone [167]. Therefore, the present study is designed to explore the feasibility of water based binder (sucrose) used as a pore forming agent in scaffold fabrication which is cost effective and also environmental friendly. It is very much convenient to fabricate scaffold with a tailored porosity and pore size [168][169]. But, the biggest challenge is that the scaffolds should afford mechanical strength which is necessary during the surgery and post surgery of a diseased part of bone.

Another possible drawback is that bacterial migration at implantation site which is a serious problem in bone related surgery, causing complication and even osteonecrosis in the injury. The bacterial migration diminishes the osteoconductivity that subsequently leads to failure of the implant [170] [69,70]. As a result the wound drainage and removal of implant needs an additional surgical intervention and causes much pain to the patients [15]. To overcome this problem, an efficient, controllable and nontoxic local drug release system is needed. Thus, it is important to consider during formulation of a bioactive materials.

Silver (Ag) is a proven versatile and effective element not only bacterial resistant agent but also a therapeutic agent [171]. However, previous studies have demonstrated that the introduction of $Ag_2O$ into bioactive glass diminishes the risk of bactericidal migration and maintaining its bioactivity [50][172–174]. Moreover, the bioactive scaffolds containing metallic ions such as $Sr^{2+}$, $Cu^{2+}$, $Ni^{2+}$ and $Co^{2+}$ act as therapeutic agents which show multifunctional properties like better osteoconductivity (new bone

growth), ability to stimulate both osteogenesis (new bone formation) and angiogenesis (for inducing vascularization) as well as antibacterial properties [11][22][12].

The bioactive glass system chosen is based on the 45S5 bioglass® composition but it has comparatively higher silica content and additional network modifiers, such as SrO and $Ag_2O$ when compared to 45S5. These constituents are playing a vital role in bone remodelling. The present study reports the mechanical behaviour, bioactivity, cell viability, proliferation, attachment, growth and bone healing as well as antibacterial properties.

## 7.2 Materials and methods

### 7.2.1 Sol-gel synthesis of bioactive glasses

For the present investigation three bioactive glass (BG) samples containing chemical composition 19 $Na_2O$ –23CaO – (5-X)SrO –50$SiO_2$ –3$P_2O_5$ (where X= 0.0, 1.0 and 3.0 mol% of $Ag_2O$) were prepared by sol-gel route as shown in **Table 7.1**. Initially, tetraethoxysilane (TEOS) (Aldrich, USA) was added into 0.1 M nitric acid and the mixture was allowed for the acid hydrolysis of TEOS for 60 min under continuous magnetic stirring at 700 rpm. Then, triethylphosphate (TEP) (Otto chemika, India) was added to it and allowed for another 30 min stirring. Another solution was prepared separately by dissolving analytical reagent grade calcium nitrate, sodium nitrate and strontium nitrate (Loba Chemie, India) in distilled water and it was added to the mixture solution with a gap of 30 min for each. The prepared solution was added slowly to the initially prepared solution and allowed for 1 h stirring. To this mixture, silver nitrate (Loba Chemie, India) was added in the dark to prevent photochemical reaction of silver. After final addition, mixing was continued for 1 h to allow the completion of hydrolysis. The silver-substituted specimen was stored and handled with utmost care in the dark to preserve the (+1) oxidation state of the silver ion. The

resultant solution was kept in a sealed PTFE Teflon container for 10 days at an ambient temperature conditions for ageing and gelation. The formed gel was placed in a sealed container and heated at 70°C for an additional 3 days period. The water was removed through small holes, which were created on the lid to allow the leakage of gases and further heat treated at 120°C for 2 days to remove all the free water. The dried gels were then calcined at 600°C for 10 h to stabilize the glass and to eliminate residual nitrates. The samples were ground with a mortar and pestle and sieved through 325 mesh sieve.

Table 7.1 Chemical composition of the sol-gel bioactive glasses (mol %).

| Glass code | $SiO_2$ | $P_2O_5$ | CaO | $Na_2O$ | SrO | $Ag_2O$ |
|---|---|---|---|---|---|---|
| **Ag-0** | 50.00 | 3.00 | 23.00 | 19.00 | 5.00 | 0.00 |
| **Ag-1** | 50.00 | 3.00 | 23.00 | 19.00 | 4.00 | 1.00 |
| **Ag-2** | 50.00 | 3.00 | 23.00 | 19.00 | 2.00 | 3.00 |

### 7.2.2 DTA/TG analysis of the sample

The differential thermal analysis (DTA) and thermogravimetric analysis (TGA) (SETARAM, France) were carried out on initial powdered sol-gel samples prepared at 120 °C in air up to 1200 °C using powdered alumina as a reference material with the heating rate of 10 °C $min^{-1}$.

### 7.2.3 The particle size and size distribution

The particle size and distribution of the sol-gel prepared bioactive glass powders (600 °C) were analyzed at 25°C. The samples were loaded into the system using water as a diluent without deflocculant. The powders were dispersed

ultrasonically and measurements were taken for a period of $10^6$ μSec for each by Beckman Coulter Delta Nano C Particle Size Analyzer (Beckman Coulter, USA).

### 7.2.4 Preparation of porous scaffold and characterization

The porous scaffold was fabricated by using bioactive glass powder and sucrose. The sucrose was employed as pore forming agent and the pore size and porosity were controlled with addition of two different ranges of sucrose particles (A and B). Thus, the sucrose (Loba Cheme, India) particles were separated into size of two ranges of size (size A =149 to 250 μm and size B =297 to 550 μm) and a mixture was prepared by mixing both of the sizes A and B of 30% and 70%, respectively. The porosity was controlled by the concentration of sucrose addition in the samples to obtain the desired porosity. Therefore, the mixture of sucrose was added (50 wt %) to sol-gelled glass powder and carboxy methyl cellulose (CMC) was used as a binder. The compound (sample + sucrose) was compacted to prepare the green pellets. The compound was uniaxially pressed in a cylindrical die of 10 mm diameter using a compaction load of 50 MPa resulting in the disc pellets and they were dried at 120 °C for 24 h. Further, the samples were sintered at 1000 $^{o}$C with a dwell time of 2 h and obtained the scaffolds. The phases present in the bioactive glass-ceramic (BGC) sample were analyzed by the powder X-ray diffractometry (XRD) (RIGAKU-Miniflex II, Japan). The porosity was measured by Archimedes' principle [9] and the pore size and microstructure were examined by using a scanning electron microscope (SEM) (Inspect S50, FEI) and the elemental analysis was done by energy dispersive spectroscopy (EDS) (Oxford Instrument, X-act, USA). The bulk specimens were coated with gold by sputter coating instrument (Hummer, USA) before their examination with SEM & EDS.

### 7.2.5 In vitro bioactivity study

The bioactivity of the BGC and Ag contained BGC samples was examined through *in vitro* test in simulated body fluid (SBF). The SBF was prepared according to Kokubo protocal [30] and that has inorganic ion concentrations similar to those of human body fluid in order to reproduce formation of apatite on bioactive materials in vitro. The SBF solution was prepared at 37 °C by dissolving reagent grade NaCl, KCl, $NaHCO_3$, $MgCl_2.6H_2O$, $CaCl_2$ and $KH_2PO_4$ into double distilled water and it was buffered at pH=7.4 with TRIS (trishydroxy methyl aminomethane) and 1N HCl. The test was performed by immersing one gram of sample in 10 ml of SBF contained in a small polyurethane container and incubated at 37 $^oC$ in a static condition for 7 days. The pH behavior of the SBF was recorded continuously for 7 days using pH meter (Universal Bio-microprocessor, India). After soaking in SBF, the sample were filtered, rinsed with double distilled water and dried in an electric air oven at 100 °C for 2 hour. The formation of hydroxy carbonate apatite layer (HCA) on the surface of the BGC samples were determined using Fourier transform infra-red spectrometry (FTIR) (Bruker Optic, Tensor-27, Germany) and the test was carried out at room temperature in the frequency range of 4000–400 $cm^{-1}$ in absorption mode for the detection of the functional groups present in the sample.

### 7.2.6 Compressive strength

The porous disc samples were subjected to compression load and the test was performed according to ASTM-C773 using Universal Testing Machine (Shimadzu, Japan) at room temperature (cross speed of 0.5 mm/min). Five samples were tested and the mean value and standard deviation was calculated. The compressive strength was calculated using the following equation (7.1):

$$\text{Compressive strength } (\sigma_c) = \frac{F}{A} \qquad -- \ (7.1)$$

Where F is the maximum compressive load during the test (N), A is the area of the specimen ($mm^2$).

### 7.2.7 Cell line growth and cell attachment

The U2OS cells ($5\times10^4$ cells/well) were seeded on the surface of the Ag-BGC scaffold and incubated for 5 days at 37°C, 5% $CO_2$ in culture medium. After 5 days of incubation at 37°C, 5% $CO_2$, the scaffold was removed, dried in air over at 100 °C for 2 h and gold coated by sputtering. The morphology and cell growth on the surface of the scaffold was observed via SEM (Zeiss, EVO 18, Germany). The elemental analysis and distribution mapping was performed using EDS (Oxford instrument, USA).

### 7.2.8 Antimicrobial study

For the bacterial culture, *E. coli* (ATCC 25922) was obtained from the American Type Culture Collection (ATCC), ATCC and clinical strains preserved at Department of Microbiology, Institute of Medical Sciences, BHU, Varanasi, India. Antimicrobial property of the Ag-0 and Ag-2 bioactive glass-ceramic scaffold samples was examined against E. coli clinical pathogen using the Kirby–Bauer disc diffusion method [175]. Mueller hinton agar (MHA) medium (Hi Media) was prepared and sterilized at 120 $^oC$ at 15 psi. The MHA plates were prepared by transferring 15 ml molten medium into sterile petri dishes. The plates were left for about 5 min to solidify and 0.1% of inoculum suspension was swabbed uniformly over the agar until the inoculums became invisible. The samples were immersed in 70% ethanol for about 3 min and then sterilized with aqueous sodium hypochlorite (4% available chlorine) for 3-5 min and then finally rinsed in sterilized double distilled water and each sample was then dried under aseptic conditions. The sterilized individual bioactive glass-ceramic discs of

Ag-0 and Ag-2 were placed in the petri dish and incubated these plates at 37 $^{o}$C for 24 h. Antibiotics like Streptomycin and Amoxicillin (10 mg $L^{-1}$) were used as positive control for gram positive and gram negative bacteria. After incubation, the plates were examined for the zone of inhibition around the discs and measured the zone formation with a measuring scale. The above study was performed in triplicate.

### 7.2.9 Platelet aggregation study

The platelet aggregation study was carried out with a 50 μL of supernatant of SBF after immersion of BGC sample for 7 days which was incubated in 250 μL of human PRP ($2.5X10^{8}$ mL) at 37 $^{o}$C for 2 min in the aggregometer (Chrono-log Co, PA, USA) with stirring at 1200 rpm. Then 10 μM Adenosine diphosphate (ADP) was added into it. Platelet aggregation was observed by measuring the change in light transmission up to 8 min after stimulation. The inhibition of platelet aggregation were expressed using Born and Wehmeier method [176] using the following equation (7.).

$$X = \frac{A - B}{A} X100 \qquad ------(7.2)$$

Where A is the maximal aggregation of platelet without bioglass and B is the maximal aggregation of platelet with bioglass sample.

### 7.2.10 *In vivo* implantation of scaffold in rat femur bone and X-ray imaging

A total of 6 male Wistar rats (body weight **250-280** g) were used in the experiment, after obtaining permission from the Institutional Ethics Committee (no. Dean/2016/CAEC/45). The Ag-2 porous scaffold sample was implanted in rat femur bone. All the animals were anesthetized by giving intraperitoneal injection of 10% sodium pentobarbital with 4 mg per kg body mass [97]. The surgical skin was shaved and disinfected with povidone iodine. A longitudinal 4.0 cm incision was made along

the femur bone. The subcutaneous tissue, muscles, and ligaments were dissected to expose the peripheral surface of the femur bone.

A large size bone defect was made by cutting a 5 mm length completely in the centre of the femur bone using a dental drill under continuous saline buffer irrigation. Ag-2 bioactive glass-ceramic scaffold sample (5 X 4 X 4 $mm^3$) was implanted in to the defect area. In order to avoid the sample and defective bone movement after implantation, the defective bone and the sample was further supported by medical grade polyethylene plate and wrapped with a wire as shown in **Figure 7.18.** The ablated tissue and skin were repositioned and sutured layer by layer and these rats were transferred to cages. X-ray radiographic images were taken by Digital X-ray radiography instrument (Shimadzu RAD speed at 41 kV) at 0, 15 and 30 days.

## 7.3 Results and Discussion

### 7.3.1 Thermal analysis of the gel glass samples

**Figure 7.1 (A-B)** shows the DTA and TG behaviors of the sol-gel prepared bioactive glass samples. It was observed from the figure that there were three major weight losses of both the samples (Ag-0 and Ag-2) observed in the temperature range from 100 $^oC$ to 1200 $^oC$ such as first weight loss which has taken place up to 150 $^oC$, second weight loss at 150 $^oC$ - 500 $^oC$ and then the third weight loss at 500 $^oC$ - 600 $^oC$. The respective weight losses are well supported with different endothermic reactions taken place in DTA curves which are revealed in **Figure 7.1 (A-B)**. First weight loss of ~25% was due to the loss of residual water which is corresponding with an endothermic peak in DTA at around 150 $^oC$. It was noticed that there was an exothermic peak at about 245$^oC$ which accompanied with no weight loss behavior. This may be due to structural change occurring in the gel (**Figure 7.1 A**). On further heating, weight loss occurred in the temperature range of 150$^oC$ to 500$^oC$ by ~15% and it is attributed to loss

of hygroscopic water and decomposition of nitrate compounds which is accompanied by an exothermic behavior. Another major weight loss of ~26% was observed in the temperature range of 500 $^{o}$C - 600 $^{o}$C which might be due to decomposition of sodium and calcium nitrates with a corresponding endothermic peak at 550 $^{o}$C. Finally, the weight loss was completed at 600 $^{o}$C in both the glasses and it remained constant up to 1200 $^{o}$C. Moreover, the glass transition temperature ($T_g$) was reported at 602 $^{o}$C and 590 $^{o}$C and the crystallization temperature (Tc) at 620 $^{o}$C and 641 $^{o}$C for Ag-0 and Ag-2 samples, respectively.

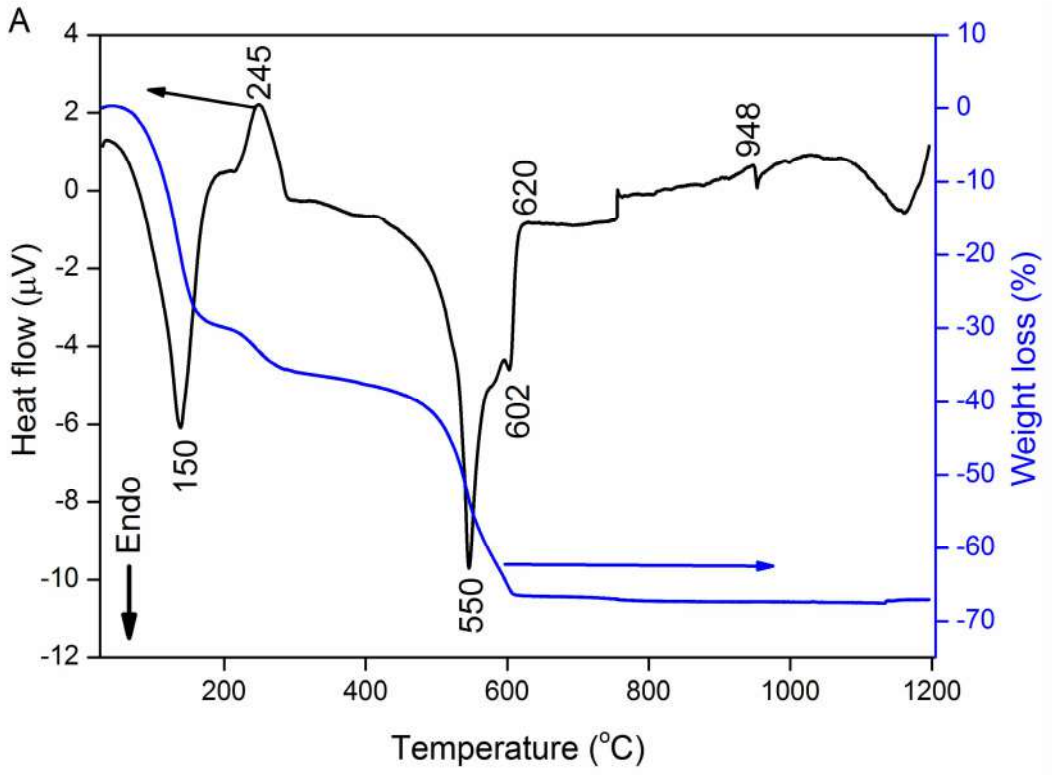

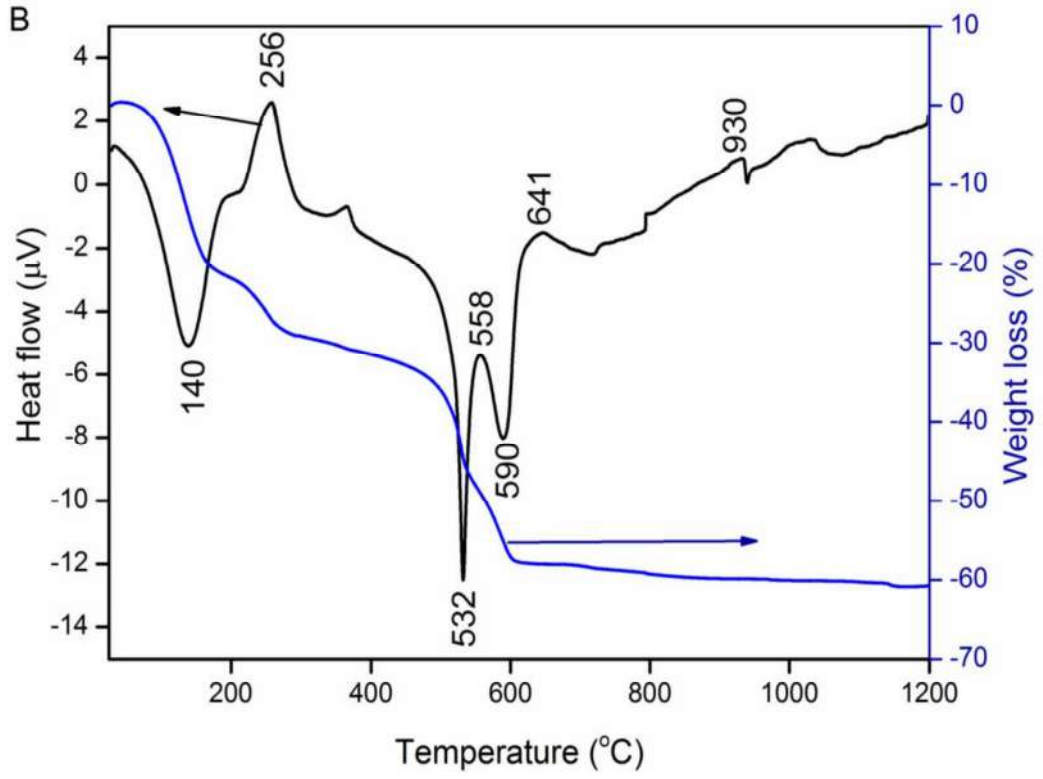


Figure 7.1 (A-B) DTA/TGA curves of sol-gel bioactive glass samples of Ag-0 (A) and Ag-2 (B), respectively.

### 7.3.2 Particle size and distribution

**Figure 7.2 (A-C)** shows the particle size and distribution of the prepared bioactive glass samples (600 °C) containing $Ag_2O$ with 0.0, 1.0 and 3.0 mol%, respectively. The mean particle size and its standard deviation was reported as (420 $\pm$ 129 nm), (1381 $\pm$ 1254 nm) and (2821 $\pm$ 2628 nm), respectively. It was noticed that the particle size increased significantly with increasing the $Ag_2O$ concentration in the BG. This might be due to the presence of $Ag^+$ ions in the system which might have agglomerated with glass particles. It was reported earlier [45] that substitution of $Ag_2O$ in the bioactive glass was distributed into ionic and metallic states in the BG. Therefore, the increase in particle size and broad spectrum of standard deviation might be due to the presence of Ag in both the states such as ionic and metallic.

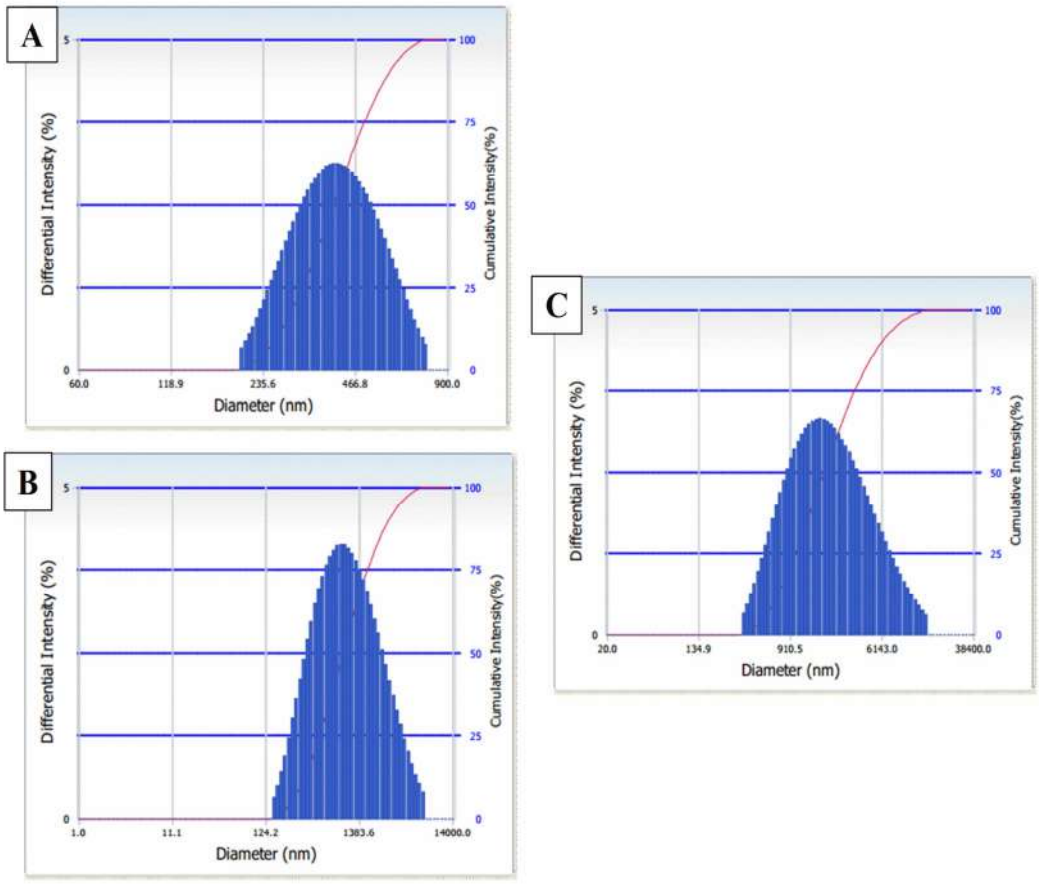


Figure 7.2 (A-C) Particle size and its distribution of sol-gel powdered bioactive glass samples containing 0.0, 1.0 and 3.0 mol% of $Ag_2O$, respectively.

### 7.3.3 XRD Analysis of the bioactive glasses

**Figure 7.3 (A-C)** shows the XRD patterns of Ag-0, Ag-1 and Ag-2 bioactive glass samples as prepared (600 $^{o}$C) and sintered at different temperatures. It was observed from the XRD patterns of the samples which show specific crystalline phases with small inconsistency in the intensity of the peaks depending on the temperatures. The Ag-0 sample as prepared has shown the amorphous state and when it was sintered at 1000 °C and the new crystalline peaks were appeared at 2θ = 33.56, 34.22, 26.34, 26.81, 23.73 and 48.71 which correspond to $Na_2Ca_2Si_3O_9$ (sodium calcium silicate) phase (**Figure 7.3 A**). The intensities of these XRD peaks were matched with the

standard JCPDS No. 22-1455. Further, these results are also in good agreement with the earlier studies carried on the sintered $Na_2O–CaO–P_2O_5–SiO_2$ and $Na_2O–CaO–SrO–P_2O_5–SiO_2$ bioactive glass-ceramic systems which have shown the similar crystalline phase[51,104,177].

The Ag-1 and Ag-2 bioactive glass samples (600 °C) show the XRD peaks at 2θ = 38.15°, 44.32°, 64.47° and 77.42° which are corresponding to metallic silver (Ag) according to JCPDS No. 89-3722 [66] [178] and it was considered as a primary crystalline phase. But, when sintered at 800 °C, additional diffraction peaks were appeared at 2θ = 33.56, 34.22, 26.34, 26.81, 23.73 and 48.71 and this corresponds to $Na_2Ca_2Si_3O_9$ (sodium calcium silicate) phase as shown in **Figure 7.3 (B-C)**. The intensities of these diffraction peaks were matched with the standard JCPDS No. 22-1455 [51,104,177]. It is interesting to note that the intensity of the primary phase (Ag phase) was found to decrease with an increase in temperature as well as increasing secondary phase voice versa. The increase in intensities of the peaks confirms the increase in the phase with temperature. Therefore, the Ag-contained bioactive glasses have demonstrated composite nature of two phases, i.e metallic silver and sodium calcium silicate phases. Thus, it might be suppressing the primary phase formation of silver and giving indications about the successful embedding of the silver metal into the glass matrix.

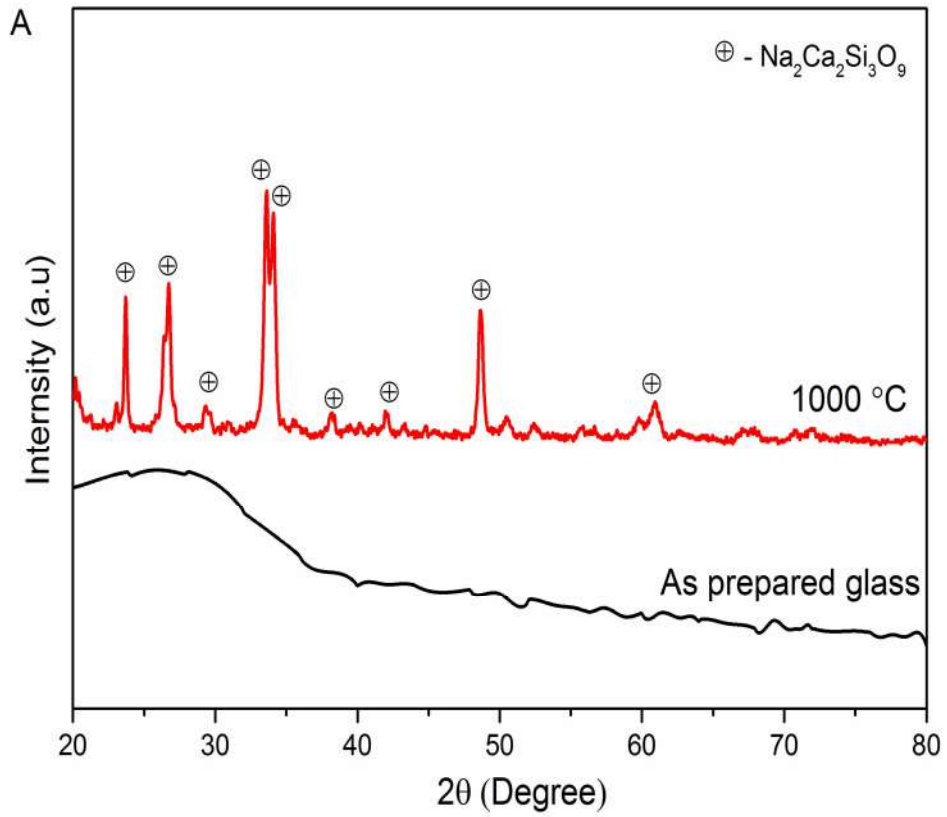
A
⊕ - $Na_2Ca_2Si_3O_9$
Internsity (a.u)
1000 °C
As prepared glass
20
30
40
50
60
70
80
2θ (Degree)

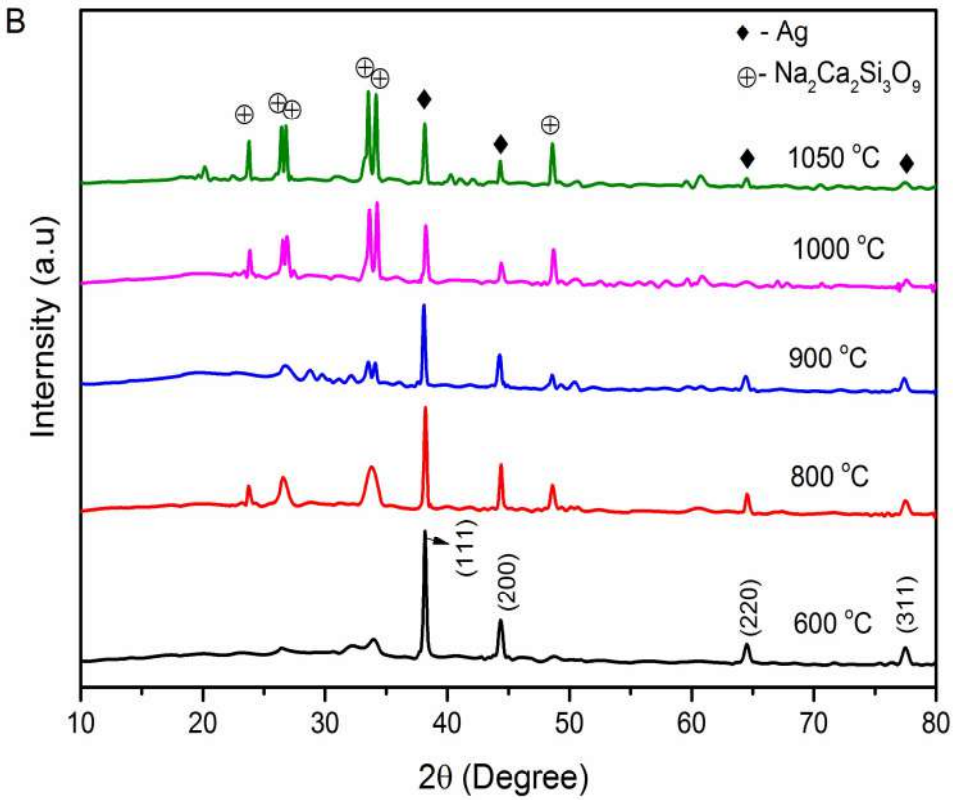
B
♦ - Ag
⊕- $Na_2Ca_2Si_3O_9$
Internsity (a.u)
1050 °C
1000 °C
900 °C
800 °C
600 °C
(111)
(200)
(220)
(311)
10
20
30
40
50
60
70
80
2θ (Degree)

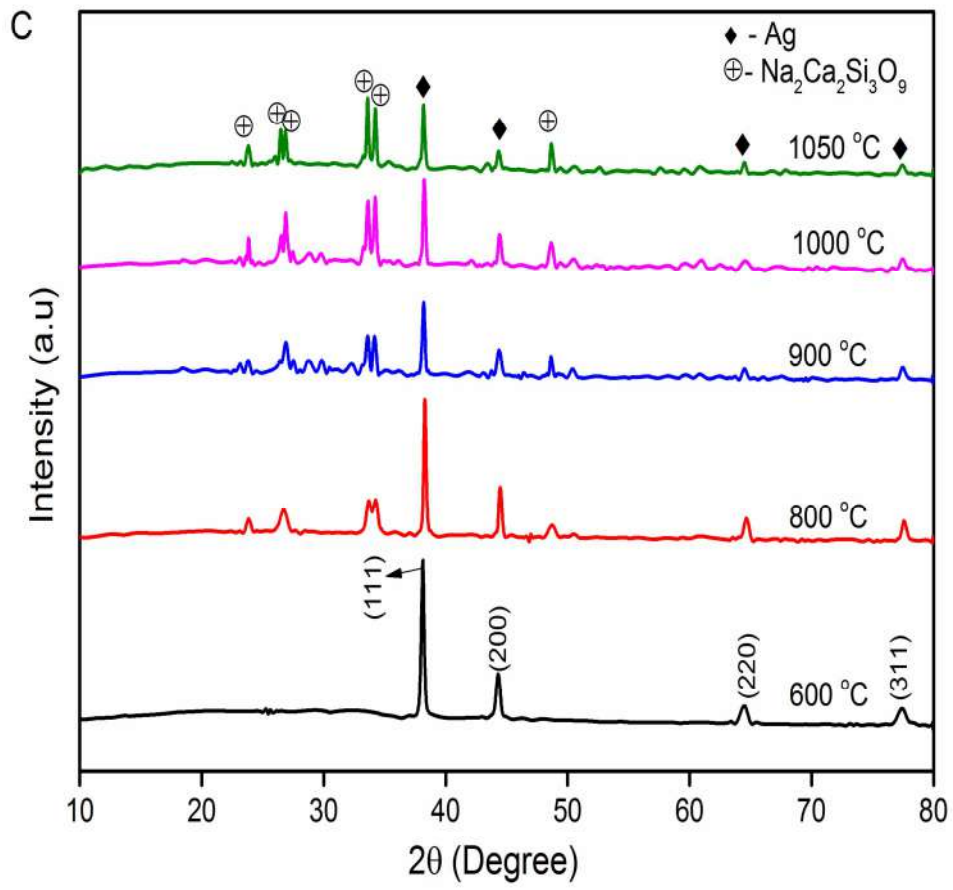


Figure 7.3 (A-C) Sol-gel bioactive glasses sintered at different temperatures (A) Ag-0, (B) Ag-1 and (C) Ag-2, respectively

### 7.3.4 Porous scaffold and microstructure of the samples

**Figure 7.4 (A-C)** shows the photographic images of the porous Ag-0, Ag-1 and Ag-2 bioactive glass-ceramic samples, respectively. The porous scaffolds were prepared with an addition of sucrose (50 wt %) in the bioactive glasses and sintered at 1000 $^{o}$C. The organic material (sucrose) was burnt out and left the pores in the structure which can be clearly seen from the photographic images. **Figure 7.5 (A)** exhibits SEM microstructure (Zeiss instrument, Germany) of the Ag-2 porous sample and it was observed from the images that different sizes of pores and bright particles have covered entire surface of the sample. The region marked on SEM image was taken for EDS

analysis as shown in **Figure 7.5 (A)**. The EDS spectra had exhibited the presence of Si, Ca, Na, P, Sr and Ag elements on the surface of the sample as shown in **Figure 7.5 (D)**. Further, these brighter rods like structure can be clearly seen at strut and pore area from the higher magnification (1000 X) of SEM images as illustrated in **Figure 7.5 (B-C)**. These brighter rods were analyzed with EDS which had confirmed the presence of silver element as shown in **Figure 7.5 (E)**. This indicates that the silver has been distributed in the whole sample. This is also in good conformance with the XRD pattern of Ag-2 sample which had shown the silver phase (**Figure 7.3 C**). Therefore, the presence of these silver rods like structure is highly beneficial in scaffolds which would strengthen the porous walls.

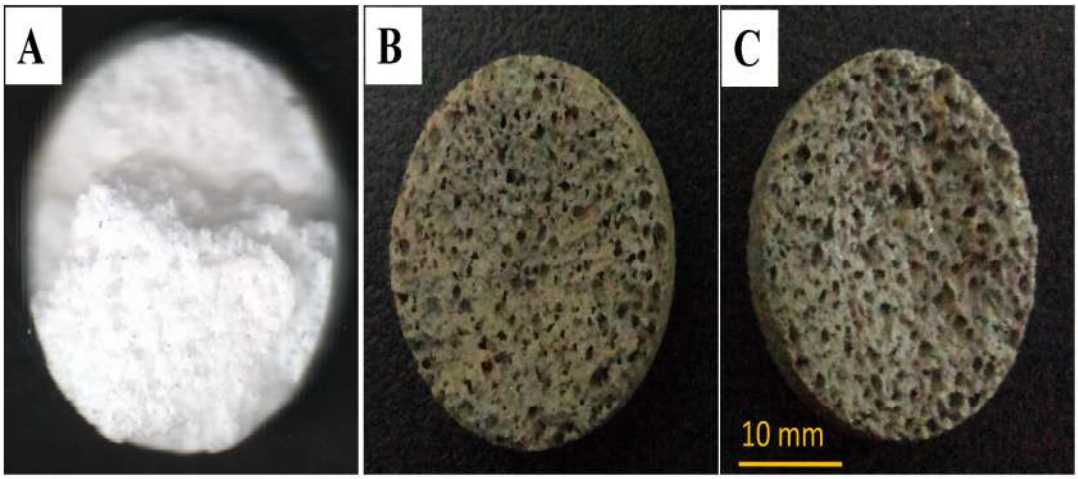


Figure 7.4 Photomicrographs of the bioactive glass samples sintered at 1000 $^{o}$C (A) Ag-0, (B) Ag-1 and (C) Ag-3.

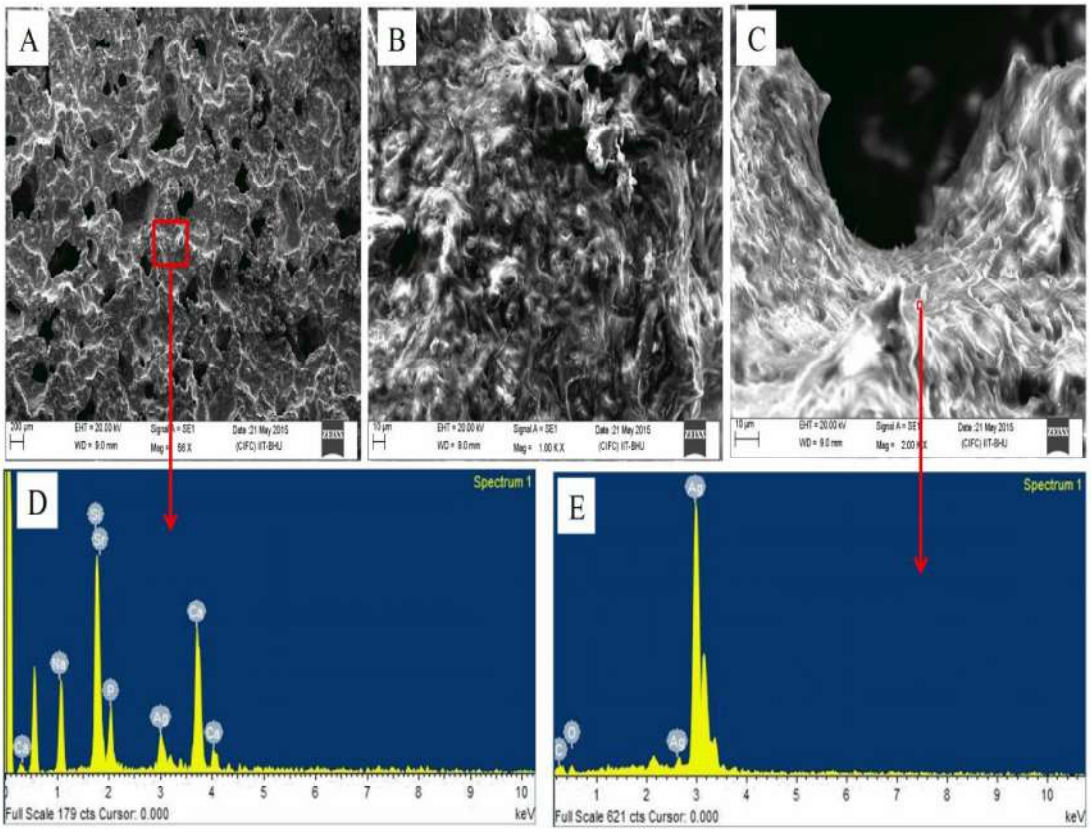


Figure 7.5 SEM micrographs of the Ag-2 bioactive glass sample sintered at 1000 $^{o}$C (A) plane surface, (B) higher magnification of strut area, (C) higher magnification of pore area, (D) EDS analysis of plane surface and (E) EDS analysis of pore area of the sample as shown by arrow mark.

### 7.3.5 Porosity and pore size

**Figure 7.6** shows the porosity of the Ag-0, Ag-1 and Ag-2 BGC samples. The porosity was achieved with an addition of 50 wt% of sucrose to bioactive glass samples and then these samples were sintered at 1000 $^{o}$C. The porosity of the samples was found to decrease from 68.33 to 57.45% with an increase in Ag concentration. This could be due to melting of silver at lower temperature during which the small pores might have closed. This clearly shows that the addition of sucrose in the sample produces the pores. It is quite obvious that the addition of pore forming agents is mostly converted into

pores after sintering. It is clearly evident from the SEM images of the Ag-2 sample which shows the pores at the plane surface (**Figure 7.7 A)**. Further the sample was cross sectioned with a diamond cutter and examined for the pores size distribution which demonstrated the presence of pores within the sample as shown in **Figure 7.7 (B)**. It can be clearly seen that the SEM microstructures of the scaffolds exhibit an inhomogeneous pore distribution but superior pore interconnectivity. SEM micrographs of the Ag-2 sample show the pores at the surface and inside as well as these pore sizes were measured at both the places by the SEM as shown in **Figure 7.7 (A-B),** respectively. It is to note that, the micrographs show the different pore sizes such as small pores and large pores as they are marked on the SEM images. The results show that the pore sizes were found to be in the range of 140 - 700 μm as measured by SEM instrument and most of the pores are fall in the range of 300-500 μm. The difference in pores is due to the mixture of two grades of sucrose particles (size A =149 to 250 μm and size B =297 to 550 μm) was used during the preparation of the sample. This clearly suggests that the addition of different grades and amount of sucrose particles can create tailored pore size and porosity, respectively. These porous scaffolds play a very important role in vascularization and cell infiltration. It was reported by earlier workers [11][162][179] that the inhomogeneous pores and shapes enhance the biointegration much faster than solid specimen *in vivo* and also suggested that the scaffolds should have the pore sizes between 300-500 μm for cell penetration, tissue ingrowth, vascularisation, and nutrient transportation for bone tissue engineering. Further, the present results of Ag-2 sample had shown the pore size mostly ranging from 300 to 500 μm. Additionally, this type of small and large pores may facilitate for vascularization and enhance the migration of osteogenic cells.

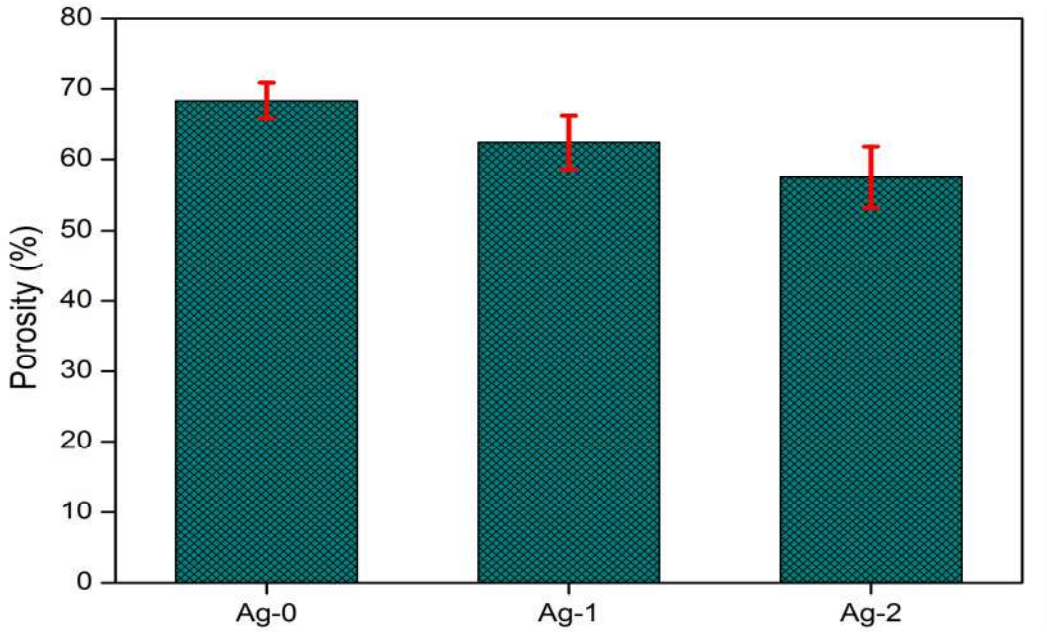


Figure 7.6 Porosity of the Ag-0, Ag-1 and Ag-2 BGC samples after sintering at 1000 $^{o}$C

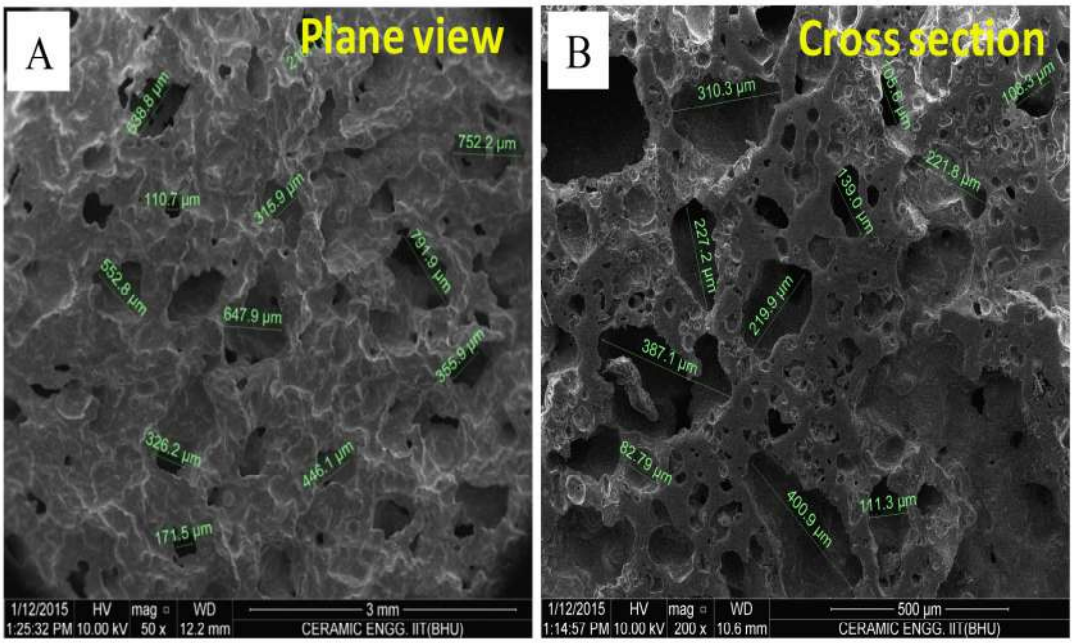


Figure 7.7 SEM micrographs of Ag-2 BGC sample sintered at 1000 $^{o}$C (A) Plane view (B) Cross section area

### 7.3.6 *In vitro* bioactivity assessment

#### A. pH behavior and mechanism of HA formation

The pH behavior of the SBF solution was measured for different time periods after immersion of the bioactive glass-ceramic samples (Ag-0, Ag-1 and Ag-2) as shown in **Figure 7.8**. All the samples possessed similar trends for their behavior. The pH was found to increase significantly from 7.4 to 8.71, 8.91 and 9.42 for Ag-0, Ag-1 and Ag-2 samples respectively on 3 day of immersion. An appreciable increase in pH demonstrates the leaching of cations from the surface of the glass which is due to the rapid release of $Na^+$ and $Ca^{2+}$ ions through the ion-exchange process with $H^+$ or $H_3O^+$ protons from the solution. In general, this increase in basicity of SBF is predictable with the first stage of Hench's mechanism [1]. The increase in hydroxyl concentration of the solution leads to attack in silicate glass network and formation of silanols which resulted in decrease in pH after 4 day. Further increase in time caused a decrease in pH which is due to the condensation and repolymerization of silica rich layer on the surface and subsequent migration of amorphous $CaO\text{-}P_2O_5$ rich film by incorporation of soluble calcium and phosphate ions from the solution [31]. However, the pH of SBF after 4 days of immersion was not significantly changed among all the samples which indicated that the cation exchange process might have reached equilibrium. Further, Greenspan and others had shown the similar behavior and changes in pH after immersion of the samples in SBF for various time periods [37,180]. Moreover, the Ag-contained bioactive glasses had shown high pH values which might be due the release of cations as well as silver into SBF. Previous studies had shown that the silver was present in ionic ($Ag^+$) and metallic (Ag) states in the bioactive glasses and thus it was released in both forms when it comes into contact with physiological solutions[64][67].

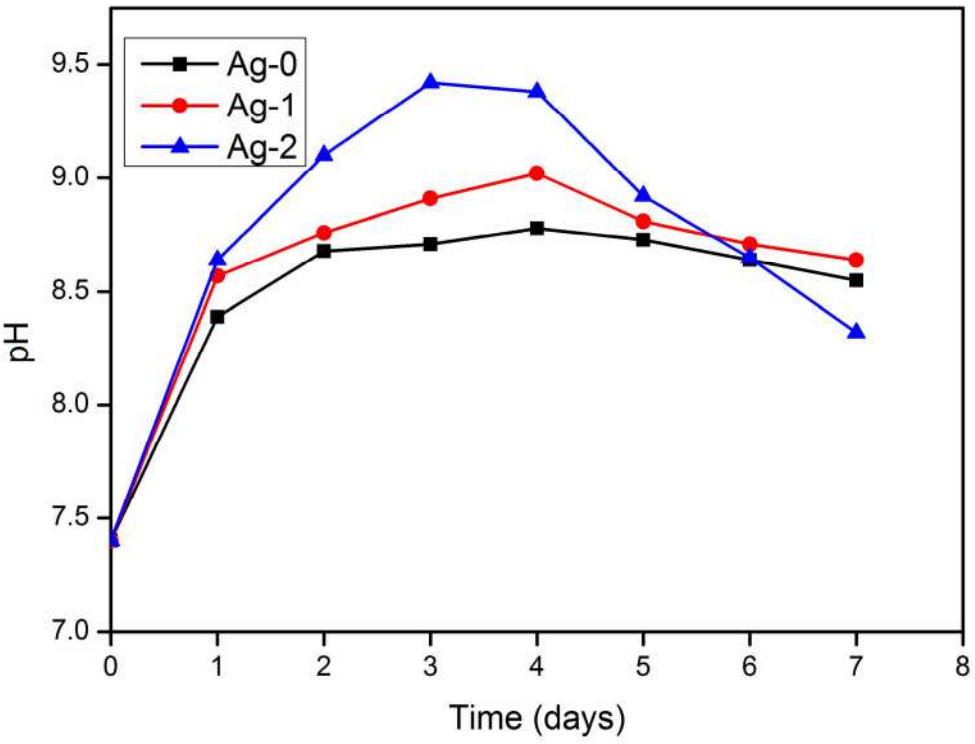


Figure 7.8 pH behavior of the SBF solution after incubation of BGC samples (Ag-0, Ag-1 and Ag-2) for different time periods

**B. FTIR spectrometry analysis**

**Figure 7.9 (A-B)** shows the Fourier transform infrared absorption spectra of the sintered bioactive glass-ceramic samples (Ag-0 and Ag-2) before and after SBF immersion, respectively. The spectra were recorded in the frequency range of 400 – 4000 $cm^{-1}$ on the FTIR spectrometer. Both the glass samples (Ag-0 and Ag-2) represent the similar trends of behavior with small change in the spectral frequencies as shown in **Figure 7.9 (A-B)**. Therefore, the functional groups discussed herewith for Ag-0 sample are represented in **Figure 7.9 (A)** The base bioactive glass before SBF treatment has revealed the frequency bands at about 446, 518, 614, 910, 1040 and 1409 $cm^{-1}$ indicating various functional groups. The resultant spectra at around 446 and 518 $cm^{-1}$ are associated with a Si–O–Si symmetric bending mode of vibration and the band at

614 $cm^{-1}$ corresponds to phosphate bending (P-O) mode of vibration (amorphous $PO_4^{3-}$). The band at 910 $cm^{-1}$ is attributed due to Si-O asymmetric stretching mode of no-bridging oxygen. Another major band at 1040 $cm^{-1}$ is associated to Si–O–Si asymmetric stretching mode of vibration. The minor band at 1409 $cm^{-1}$ is attributed due to $CO_3$ groups.[173][109].

**Figure 7.9 (A - B)** also shows the new infrared spectral bands of the Ag-0 and Ag-2 BGC samples after immersion in SBF for 1, 3, 5 and 7 days. After 1 day immersion in SBF, the new bands were found to appear at wavenumbers 570, 658, 785, 947, 1409 and 3682 $cm^{-1}$ in Ag-0 BGC sample as well as 550, 645, 790, 1405 and 3750 $cm^{-1}$ in Ag-2 BGC sample. It was found that these frequency bands are identical to each other. Therefore, the substitution of $Ag_2O$ in the BG did not affect the functional groups appreciably. The major bands appeared at around 570 and 658 $cm^{-1}$ correspond to (phosphate) P-O bend crystalline which is regarded as major characteristic peaks of crystalline HA. The band at 910 $cm^{-1}$ has shifted to higher frequency at 947 $cm^{-1}$. The bands at 785 and 1409 $cm^{-1}$ are due to the presence of carbonate (C-O) stretching mode of vibration. Another band at 3682 $cm^{-1}$ is assigned due to the presence of O-H groups. The new bands emerged after immersion of the sample in SBF is favorably due to the formation of hydroxyl carbonate apatite (HCA) layer. The infrared frequencies and related functional groups were found to match with the earlier reports of the previous workers [37,181].

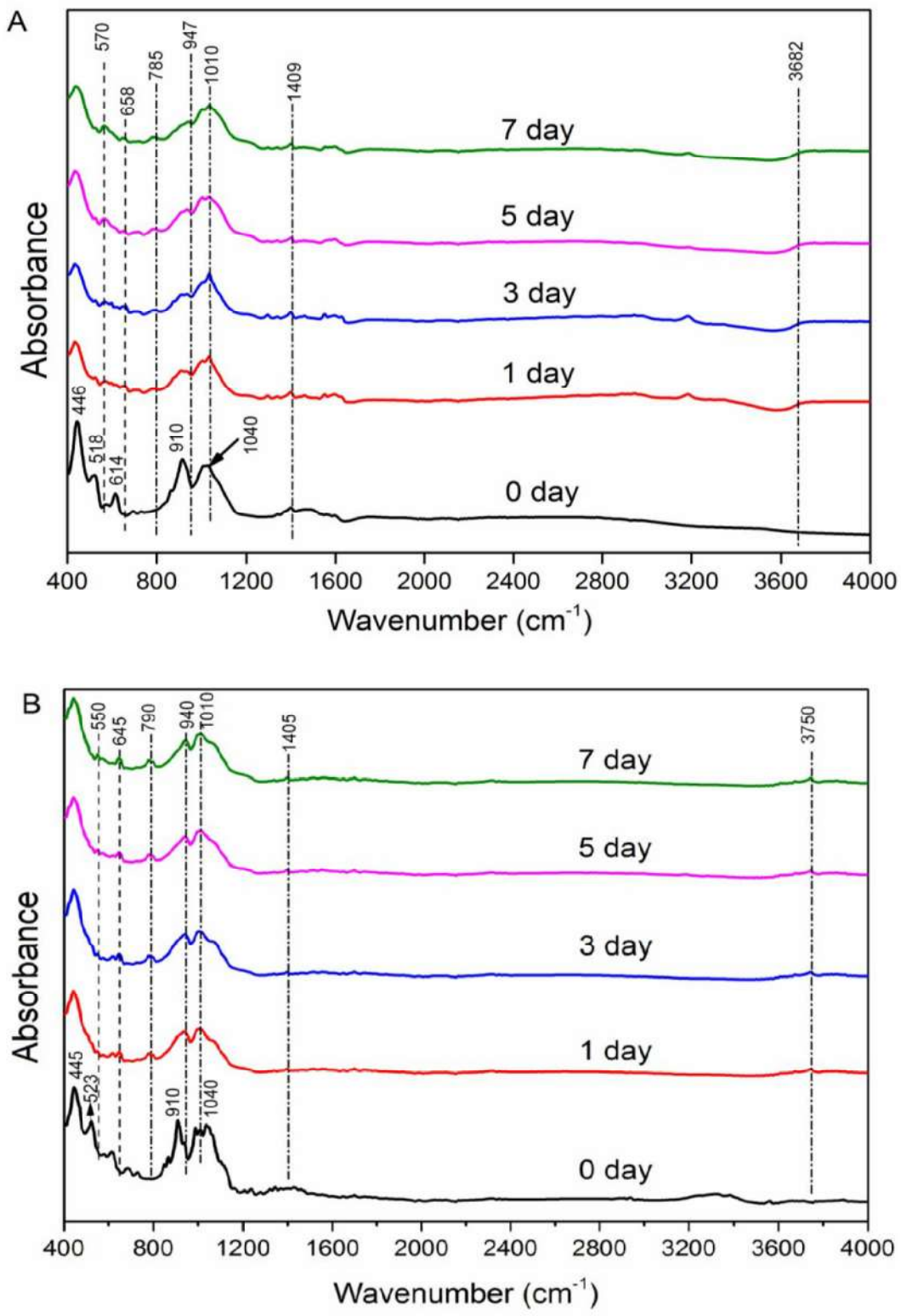


Figure 7.9 FTIR spectra of (A) Ag-0 and (B) Ag-2 bioactive glass-ceramic samples before and after immersion in SBF for different time periods

## C. XRD analysis

**Figure 7.10 (A-C)** shows the XRD patterns of the sintered bioactive glass-ceramic samples (Ag-0, Ag-1 and Ag-2) before and after immersion in SBF for different time periods. The results show the formation of crystalline phases after SBF treatment. In general, the bioactivity of the sample is associated with the ability of hydroxy apatite (HA) layer formation on their surface in SBF under physiological conditions. The *hkl* planes (211), (203) and (313) are located at 2θ degree corresponding to crystalline phase of hydroxy apatite [$Ca_{10}(PO_4)_6(OH)_2$] and these diffraction peaks were matched with the standard JCPDS No. 74-0565 [95,131]. Therefore, all the samples have confirmed the HA phase formation after immersion in SBF for 7 days.

The Ag-0 BGC sample had shown the sodium calcium silicate phase as a major crystalline phase as compared with HA after 7 days of immersion in SBF. It is interesting to note that Ag-1 and Ag-2 BGC samples had exhibited HA as a main crystalline phase as compared to silver and sodium calcium silicate phases after SBF treatment as shown in **Figure 7.10 (B &C)**. In Ag-1 and Ag-2 BGCs, the HA phase was more prominent as compared with Ag-0 BGC sample and the $Na_2Ca_2Si_3O_9$ has disappeared after immersion in SBF for 7 days. Moreover, the silver phase was still present in Ag-1 and Ag-2 BGC samples even after SBF treatment. It was also observed that the silver peak at 2θ around 38.4$^o$ was found to decrease with increasing in immersion time which might be due to the release of silver ions from the samples. Newby et al [171] had demonstrated that the presence of silver in the bioactive glass scaffold had not inhibited the formation of HA in SBF. Moreover, in the present investigation the substitution of $Ag_2O$ in the base composition had improved the

bioactivity as compared to Ag-0. Thus, the Ag–contained bioactive glass-ceramic samples had demonstrated enhanced bioactivity and HCA phase formation.

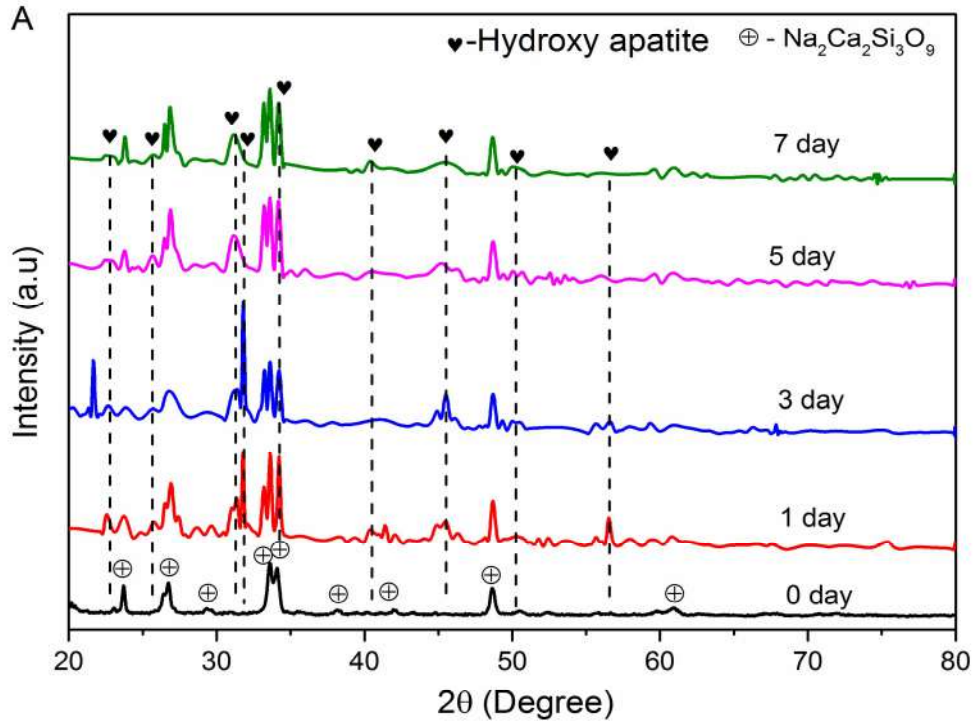


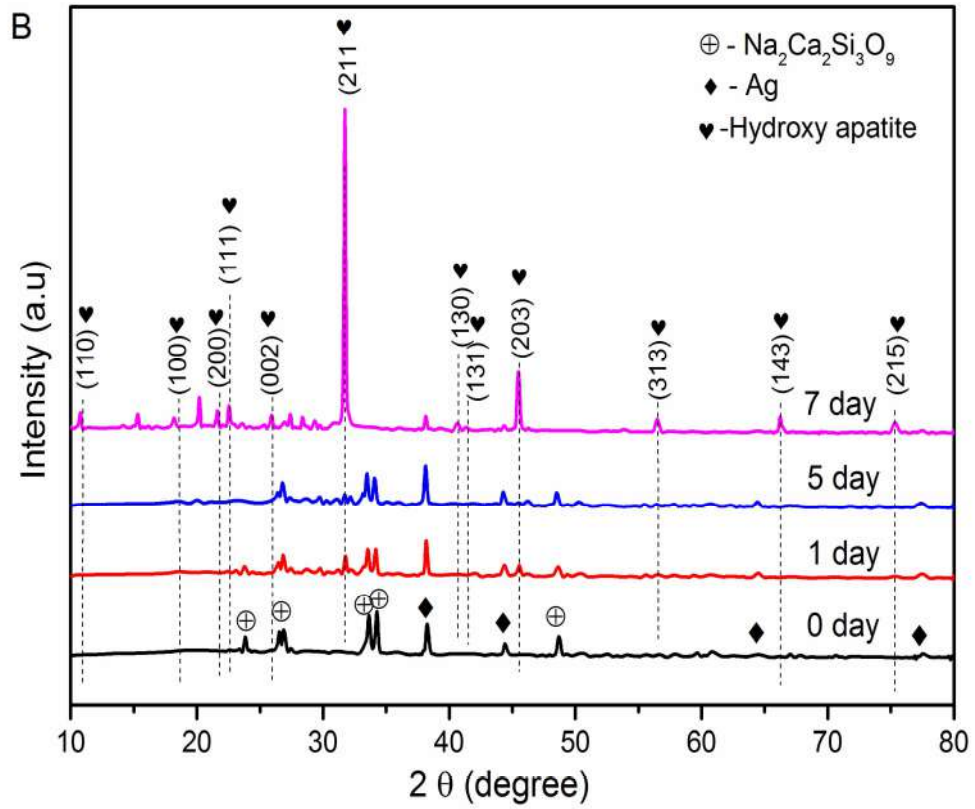

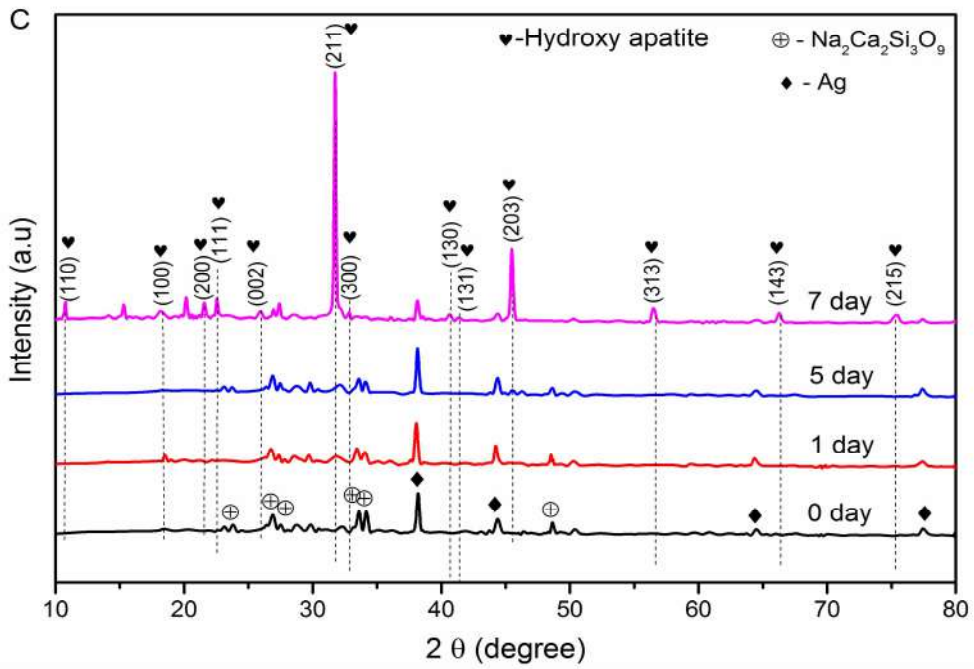


Figure 7.10 XRD patterns of (A) Ag-0, (B) Ag-1 and (C) Ag-2 bioactive glass-ceramic samples before and after immersion in SBF for different time periods

### D. Surface morphology before and after SBF treatment of the samples

**Figure 7.11 (A-B)** shows the SEM (Inspect S50, FEI) micrographs of the Ag-0 and Ag-2 sintered bioactive glass-ceramic samples before SBF treatment, respectively. Ag-2 sample presents the better sintered nature of the surface as compared with Ag-0 BGC due to the presence of silver which might have acted as a flux in the glass. **Figure 7.11 (C-D)** shows the SEM images of the Ag-0 and Ag-2 bioactive glass-ceramic samples after immersion in SBF for 7 days. A significant change in surface morphology was seen when compared with the initial surface of the samples. The SEM micrographs represent that spherical particles (bone like structure) have covered the entire surface of the samples with variable shape and size. The newly developed crystals on the surface of the bioactive glasses were assumed to be hydroxy carbonate apatite [61][64]. This is in good conformance with XRD patterns of these samples which had shown HCA

crystalline phase after immersion in SBF (**Figure 7.10 A & C**). Furthermore, it is interesting to note that the Ag-2 BGC sample exhibits the presence of metallic silver phase even after SBF treatment and it can easily be differentiated from the surface of the sample (**Figure 7.11 D**). This is in good agreement with the XRD pattern of Ag-2 BGC sample (**Figure 7.10 C**).

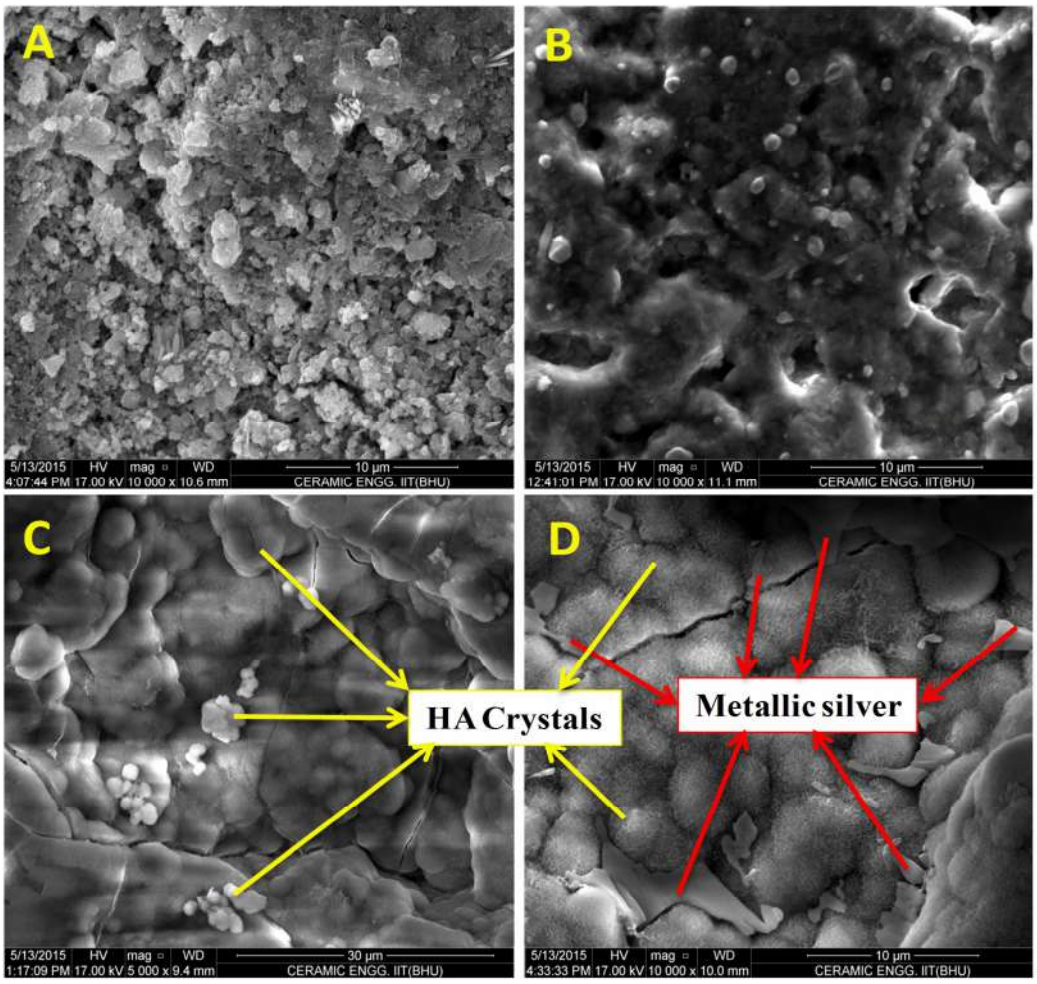


Figure 7.11 SEM micrographs of the surface of bioactive glass-ceramic sample surface before immersion in SBF (A) Ag-0 BGC, (B) Ag-2 BGC and after immersion in SBF for 7 days (C) Ag-0 BGC and (D) Ag-2 BGC representing the HA crystals and metallic silver.

### 7.3.7 Compressive strength

**Figure 7.12** shows the compressive strength of the porous bioactive glass-ceramics samples which were sintered at 1000 $^{o}$C. In general, the mechanical strength of a porous sample mainly depends on the existence of solid content in the porous matrix. Therefore, the porosity plays an important role in mechanical properties of the materials as the porosity increases the mechanical strength decreases. The present results demonstrate that the compressive strength has been found to increase from 2.4 to 18.3 MPa with increasing concentration of Ag as shown in **Figure 7.12**. It was reported earlier that the compressive strength of cancellous bone is in the range of 2 - 12 MPa [74,111]. The significant improvement in the compressive strength might be due to the reinforcement of silver nano rods in the glass-ceramic matrix. It is in good support with XRD and SEM analysis data which had shown the silver nano particles embedded on the matrix as shown in **Figure 7.3 (C)** and **Figure 7.5 (A-C)**, respectively. The Ag phase was present in the bioactive glass sample sintered at 600 $^{o}$C as shown in **Figure 7.3 (C)**, as the temperature increases the Ag phase was found to decrease. This suggests that Ag was embedded in the glass matrix which has resulted in higher mechanical strength. Previously Fu et al. [182] prepared bioactive glass (13–93) scaffolds with oriented microstructures and reported the compressive strength (25 ± 3) MPa and porosity 55–60% with pore width of 90–110 μm of the columnar scaffolds. Another study by Xin Liu et al [166] reported the porosity as (50 ± 4)% with a average pore diameter of 100 μm and demonstrated the compressive strength as (47 ± 5) MPa. Tarafder et al [183] had reported the compressive strength in the range of 4.7-12.01 MPa with the pore size in the range of 361-716 μm and porosity of 42-50%. In the present study, the compressive strength and porosity results are comparable with the

previous worker's results. Therefore, the substitution of Ag in the bioactive glass has increased the compressive strength significantly as compared to Ag-free sample.

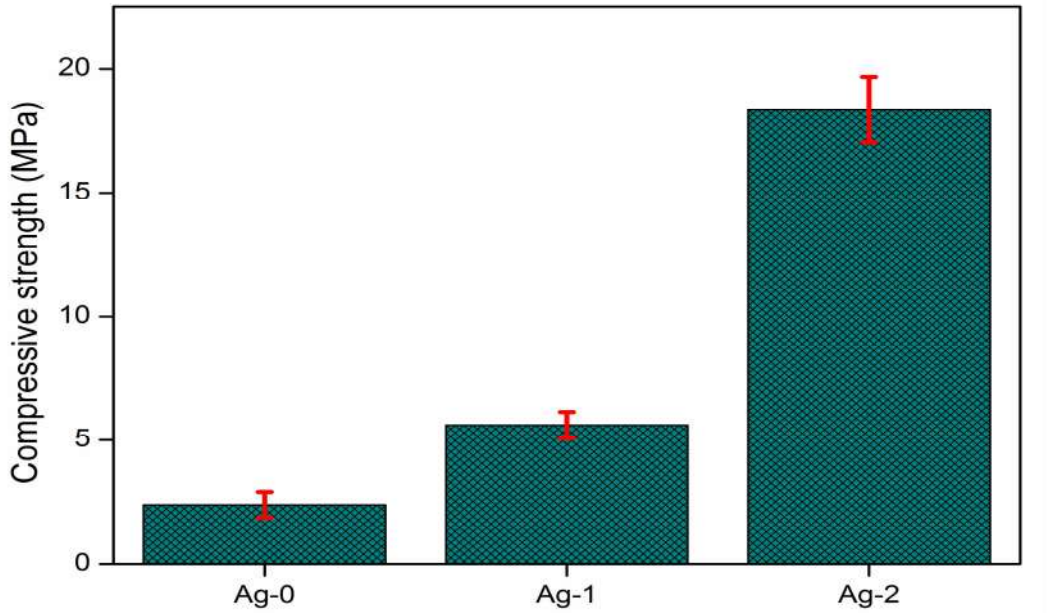


Figure 7.12 Compressive strength of Ag-0, Ag-1 and Ag-2 samples after sintering at 1000 $^{o}$C

### 7.3.8 *In vitro* cell culture studies

**A. Cell viability, cytotoxicity and proliferation**

The *in vitro* biocompatibility of the Ag-0, Ag-1 and Ag-2 bioactive glass-ceramic samples was assessed by using human osteosarcoma (U2-OS) cell lines. The cell viability, cytotoxicity and proliferation investigations were carried out with different quantities (50, 100, 250 and 500 mg/ml) of the samples against the U2-OS cell lines as shown in **Figure 7.13 (A-C)** respectively. Viability of only tumour cells treated with medium alone was considered as 100%. The samples revealed significant viability towards the osteosarcoma cell lines after 48 h of incubation at different concentrations (mg/ml) of the sample. It was observed that the cell viability was found to decrease as the concentration of the sample increased in all cases. However, the viability was not

significantly affected even at higher concentration (500 mg/ml) of Ag-2 BGC sample and these results are comparable with the Ag-0 BGC sample. The superior cell compatibility might be due to the presence of sodium calcium silicate crystalline phase in the samples which was confirmed by XRD as shown in **Figure 7.3 (A-C)**. Previous investigations have also demonstrated that the sodium calcium silicate and silver phases are biocompatible materials [163,184,185][186][187]. Therefore, our results imply that the cell viability was not affected significantly by the samples. The cytotoxic effect of the sample against U2-OS cell line is shown in **Figure 7.13 (B)**. The data suggest that the sintered bioactive glass-ceramic samples were non toxic to the U2OS cell lines even after 48 h. The Ag-2 bioactive glass-ceramic sample shows insignificant cytotoxicity (25.9%) at higher concentration (500 mg/ml). However, these results are comparable with the Ag-0 BGC sample. Thus, the cell viability and cytotoxicity data suggest that prepared bioactive glass-ceramic scaffold samples are tolerant to U2-OS cells and hence biologically compatible. Further, the cell proliferation assay was carried out using U2OS cell lines cultured with different concentrations (50, 100, 250 and 500mg/ml) of the samples for 48 h. The cells were found to grow in the presence of all the samples after 48 h of incubation period at all the concentrations in the range as shown in **Figure 7.13 (C)**. It was observed that the cell proliferation was found to decrease as the concentration of the samples increased. It is quite obvious that the sample to culture medium ratio has increased. Furthermore, the amount of ions released from the sample has not affected significantly on the cell viability, cytotoxicity and proliferation. Therefore, the results suggest that substitution of $Ag_2O$ in the base glass is not harmful to the cell lines and also demonstrate cell cytocompatibility.

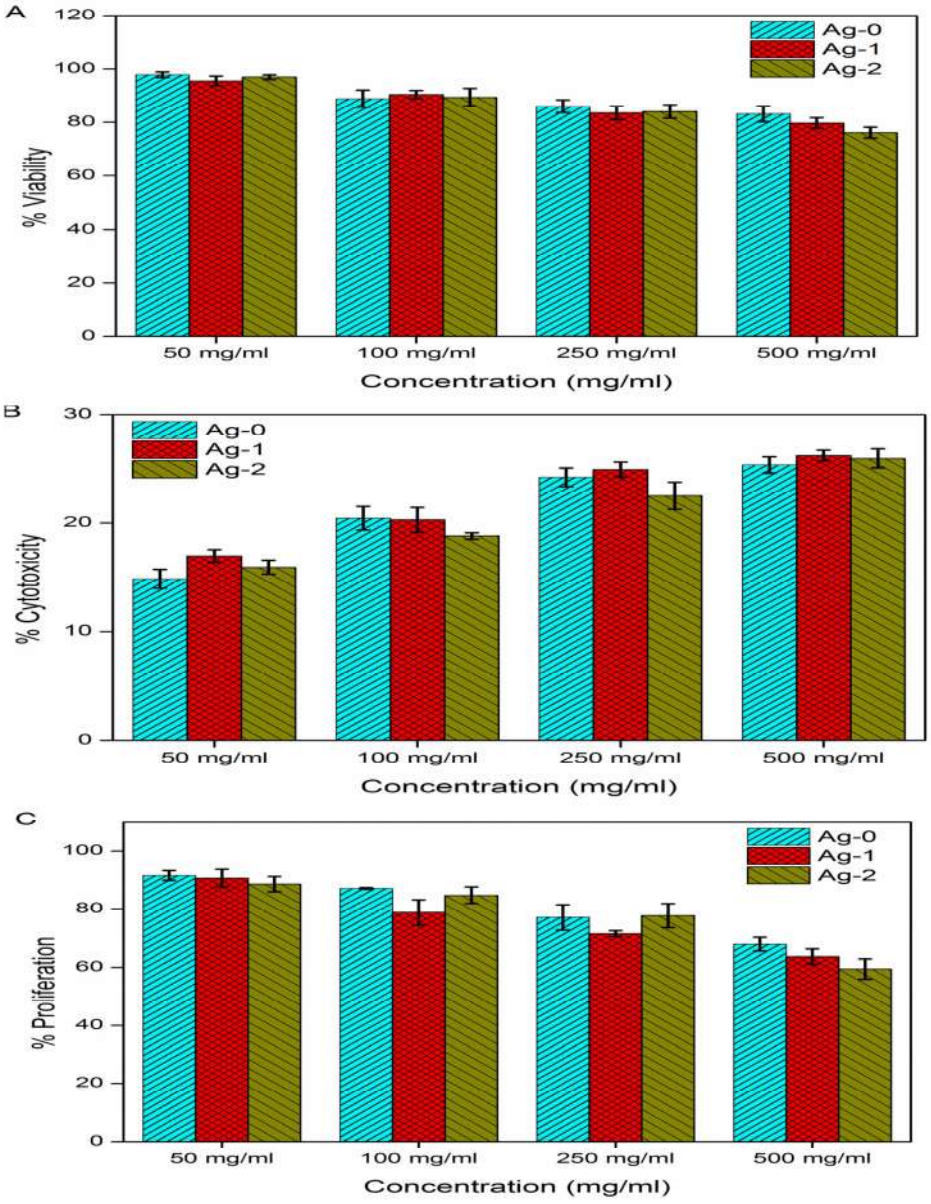


Figure 7.13 *In vitro* cell culture investigation results of the Ag-0, Ag-1 and Ag-2 bioactive glass-ceramic samples with different concentrations (50, 100, 250 and 500 mg/ml) (A) Cell viability, (B) Cell cytotoxicity and (C) Cell proliferation

**B. Detection of cell apoptosis**

Qualitative evaluation of cell apoptosis has been carried out in the presence of Ag-0, Ag-1 and Ag-2 bioactive glass-ceramic samples. The release of ions from the sample into the body fluids sometimes may lead to change in cell morphology which

may further cause cell death. Therefore, apoptosis was determined by monitoring changes in the cell size and externalization of phosphatidylserine of the U2OS cells. **Figure 7.14** shows the fluorescence images of cell morphology after incubation of the samples with U2OS cell lines for 8 h. It may be reasonable to consider that the inhibitory activity of the samples sometimes may cause cytotoxic effect. The fluorescence images have demonstrated that these samples did not cause cell apoptosis. However, Ag-0 BGC sample shows some red spots in comparison with Ag-1 BGC and Ag-2 BGC samples. Hence, the qualitative results further support that substitution of $Ag_2O$ in the base bioactive glass sample has not caused cell death.

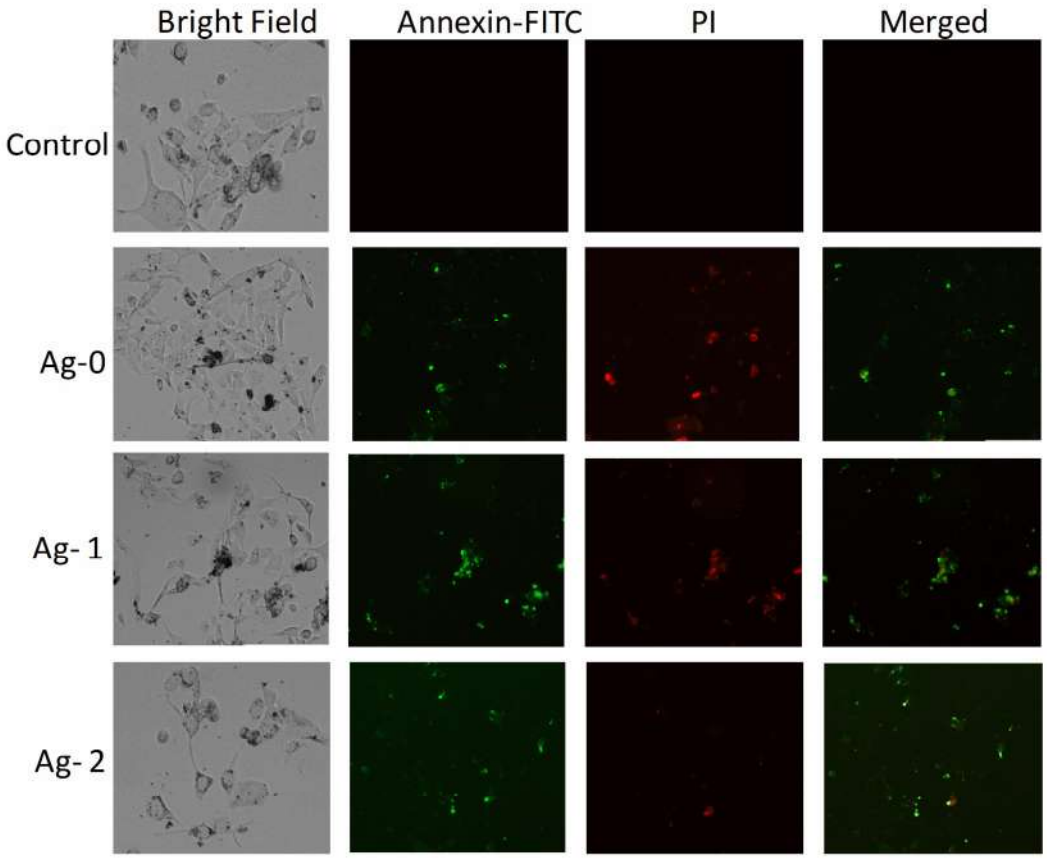


Figure 7.14 Florescence microscopic analysis of induction of cell apoptosis caused by Ag-0, Ag-1 and Ag-2 bioactive glass-ceramic samples after 8 h of incubation

## C. Cell attachment and growth

The *in vitro* osteoconductivity of osteosarcoma cells on the Ag-2 bioactive glass-ceramic porous scaffold has been evaluated in terms of cell adhesion and growth. In order to check the cell interaction with the sample and attachment on the surfaces, the U2-OS cells were cultured on the porous discs of the Ag-2 sample and incubated for 5 days at 37$^{o}$C. After incubation, the Ag-2 scaffold sample was taken out of the culture plate and washed with PBS to remove the unattached cells and the sample was dried and then examined with SEM & EDS. The U2-OS cells were found to grow significantly on the surface and pore area of the disc after 5 days of culture as shown in **Figure 7.15 (A)**. Further, it can be clearly seen from the higher magnification images (**Figure 7.15 B-D**) that the cell attachment and growth were apparent not only at the surface but also at pore area (**Figure 7.15 C)** and wall area as shown in **Figure 7.15 (D)**. It indicates that the growth of the cells was taking place on 3D structured porous sample and these pores are sealing with the newly developed HCA layer. This significant growth could be attributed due to osteogenic differentiation of osteoblast like cells. Thus, the bone is continuously remodelling in a dynamic process where cell differentiation takes an active role for the formation of new bone and this effect could be evidently seen on walls of the sample. Further, the EDS analysis was also performed to assess the composition of the crystals on the surface of the scaffold (**Figure 7.15 E**). The EDS spectra show the presence of Ca, P, Na, Sr, Ag and Si elements, while Ca and P are apparently higher in concentrations in comparison to other elements which confirm the new bone (Ca-P) formation. This is also in good conformance with elemental mapping results which was done over the surface of the Ag-2 scaffold as shown in **Figure 7.16**. It was observed that there is presence of Ca, P, Si, Na, Ag and Sr ions which were evenly distributed over the sample. Further, the $Ca^{2+}$ and $PO_4^{3-}$ ions

were more prominent in comparison to other ions. This is further supports that the surface is rich in HCA layer. It is interesting to note that the $Ag^{+}$ ions were found on the entire surface of the sample even after 5 days of culture, while Sr ions were comparatively less in numbers. This indicates that the release of Ag ions might be slow and Sr might be high.

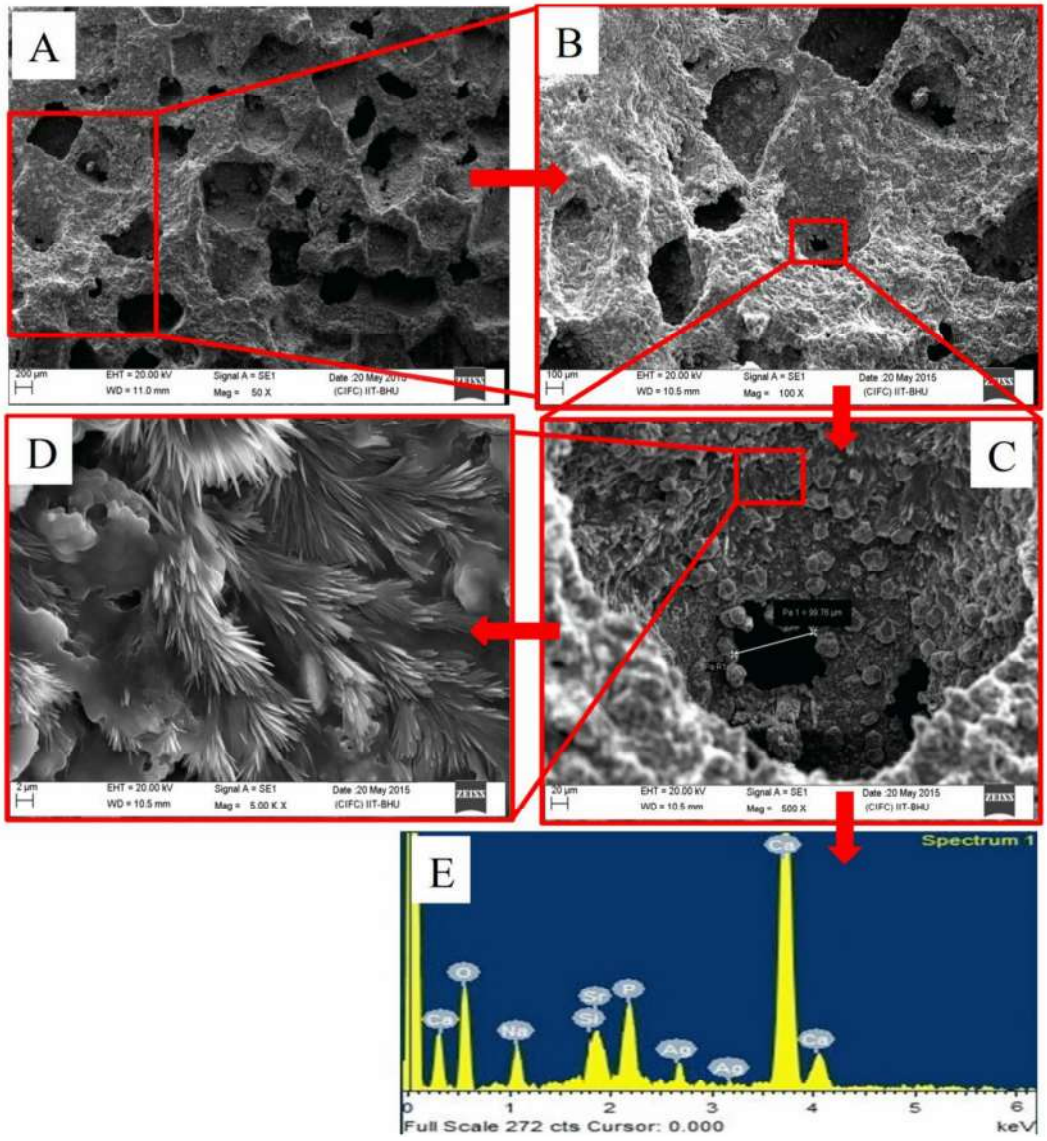


Figure 7.15 (A) Cell attachment and growth on the porous Ag-2 sample (B) higher magnification, (C) Pore area and (D) Pore wall area at higher magnification as well as (E) EDS spectra of the sample.

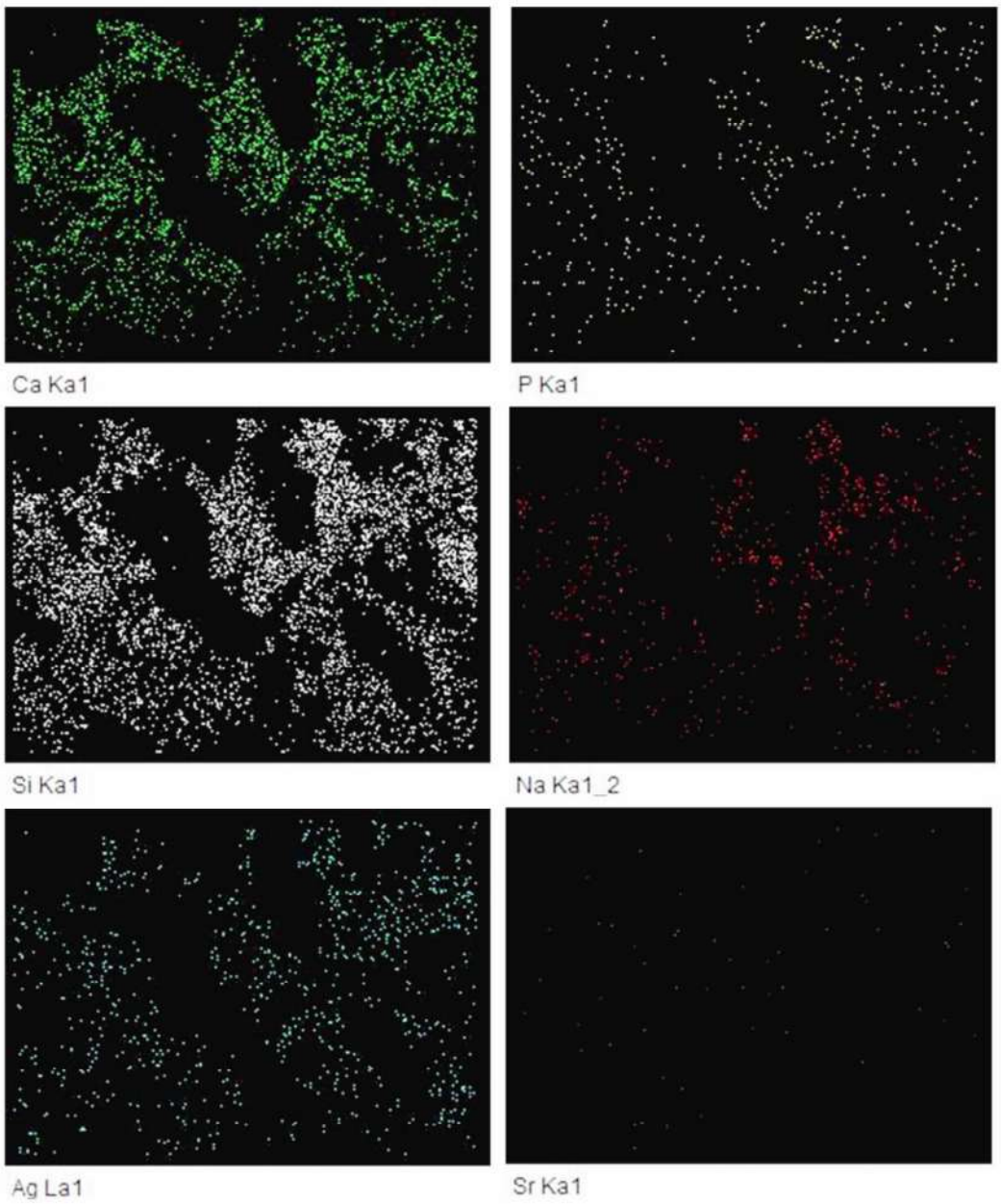


Figure 7.16 Elemental mapping of Ag-2 scaffold sample after cell culture exhibiting the concentration and distribution of Ca, P, Si, Na, Ag and Sr ions.

### 7.3.9 Blood compatibility studies

**A. Hemolysis, WBC viability, RBC integrity and size distribution**

Hemolysis takes place when the red blood cells come in contact with the implant materials. Therefore, this study is very important before the use of the implant. Hemolysis is the breakage of the red blood cells (RBC) membrane causing the release of the hemoglobin and other internal components into the surrounding fluids. It has been well described that the permissible limit of hemolysis for biomedical implants should be less than 5% [95,188]. It can be clearly seen from the **Figure 7.17 (A)** that the bioactive glass-ceramic samples (Ag-0 and Ag-2) did not affect RBC with respect to hemolysis data. The % hemolysis was determined in the presence of the sample and found that the results did not exceed the control value of 5%. Further, hemolysis studied at increasing incubation time point demonstrates partial hemolysis as compared to initial test time of 30 min, but it did not cross the limit of 5% even after 2 h of contact with blood (**Figure 7.17 A**). Thus, this suggests that these samples were relatively tolerant to the RBC and can be considered as non-hemolytic. Furthermore, fresh peripheral blood mononuclear cell (PBMC) from normal donor was taken and examined for the effect of the Ag-0 and Ag-2 BGC samples on the PBMCs. It was observed that the PBMCs also remained unaffected by these samples with no significant loss of viability even at all the concentrations investigated **(Figure 7.17 B)**. The substitution of $Ag_2O$ in the BG has not significantly affected the white blood cells (WBC) and it is comparable with the Ag-0 BGC sample. **Figure 7.17 (C)** shows the microscopic images of RBC after incubation with the Ag-0 and Ag-2 BGC samples for 4 h. The micrograph images exhibit no change in RBC cell morphology even after 4 h of incubation with the samples and it is comparable with the control as a reference without sample. It was also observed that there was no accumulation of cells (RBC).

Therefore, the results imply that these samples were compatible with the major components of the blood such as RBC and WBC as well as they were non-hemolytic.

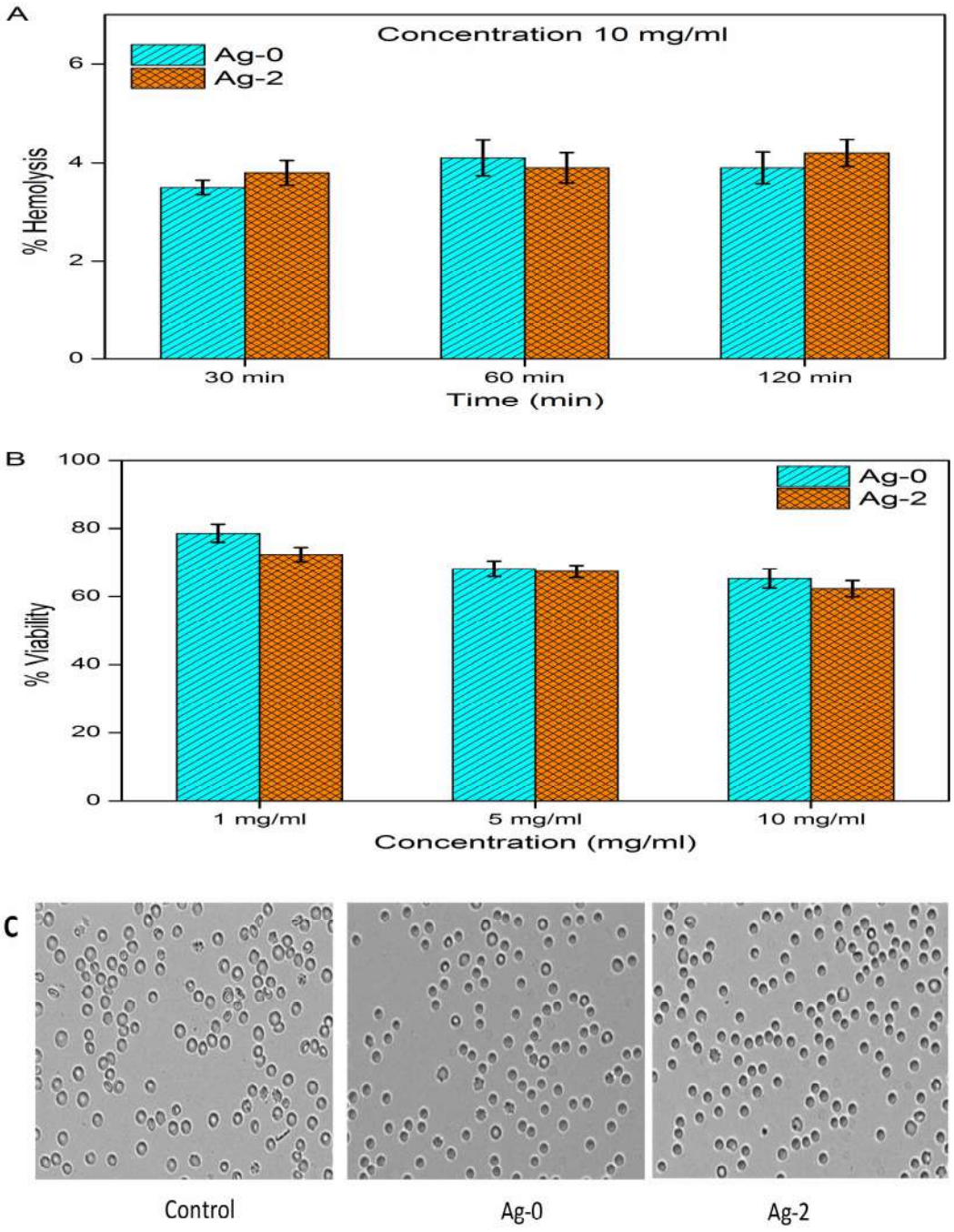


Figure 7.17 (A) Percent hemolysis caused by Ag-0 and Ag-2 bioactive glass-ceramic samples after incubation for different time periods, (B) Viability of blood peripheral mononuclear cell (PBMC) after incubation at different concentrations and (C)

Microscopic images of Ag-0 & Ag-2 on RBC after 4 h incubation with 10mg/ml concentration (20X magnification)

**B. Thrombus formation (blood platelet aggregation)**

It was observed from the pH study that the ions were released from the surfaces of the samples after immersion in SBF (**Figure 7.8**). Therefore, the amount of ions released from the sample might have entered into the human body fluids when implanted. This may cause sometimes platelet aggregation which involves blood coagulation due to the adhesion of platelets to fibrinogen, collagen and to implant surface and thus forms blood clots (thrombus formation). In order to examine the effect of ions released from the sample on the platelets and its coagulation behavior, the supernatant of the SBF was taken out after immersion of the samples (Ag-0 and Ag-2 BGC) for 7 days and incubated with platelet rich plasma (PRP) ($2.5X10^8$ mL). **Figure 7.18 (A)** shows the change in % light transmittance with respect to time after incubation of supernatant of SBF of Ag-0 and Ag-2 BGC samples with PRP. It can be seen from the image that the Ag-0 sample shows light transmittance of around 80% after 8 min, whereas the Ag-2 BGC sample had shown a lesser value of around 51%. Further, **Figure 7.18 (B)** shows the percent platelet aggregation caused by the samples after 8 min of incubation. It was found that the sample (Ag-2 BGC) containing $Ag_2O$ had shown more than 40% of inhibition while Ag-0 had revealed around 4%. This is in good conformance with earlier investigations carried out by Shrivastava et al [189], who had shown that the nano silver prevents the platelet adhesion to fibrinogen and collagen without conferring any lytic effect on them. Therefore, the substitution of $Ag_2O$ in BG has a significant benefit in comparison to Ag-free sample as it inhibits the blood coagulation and hence prevents the thrombus formation in the body.

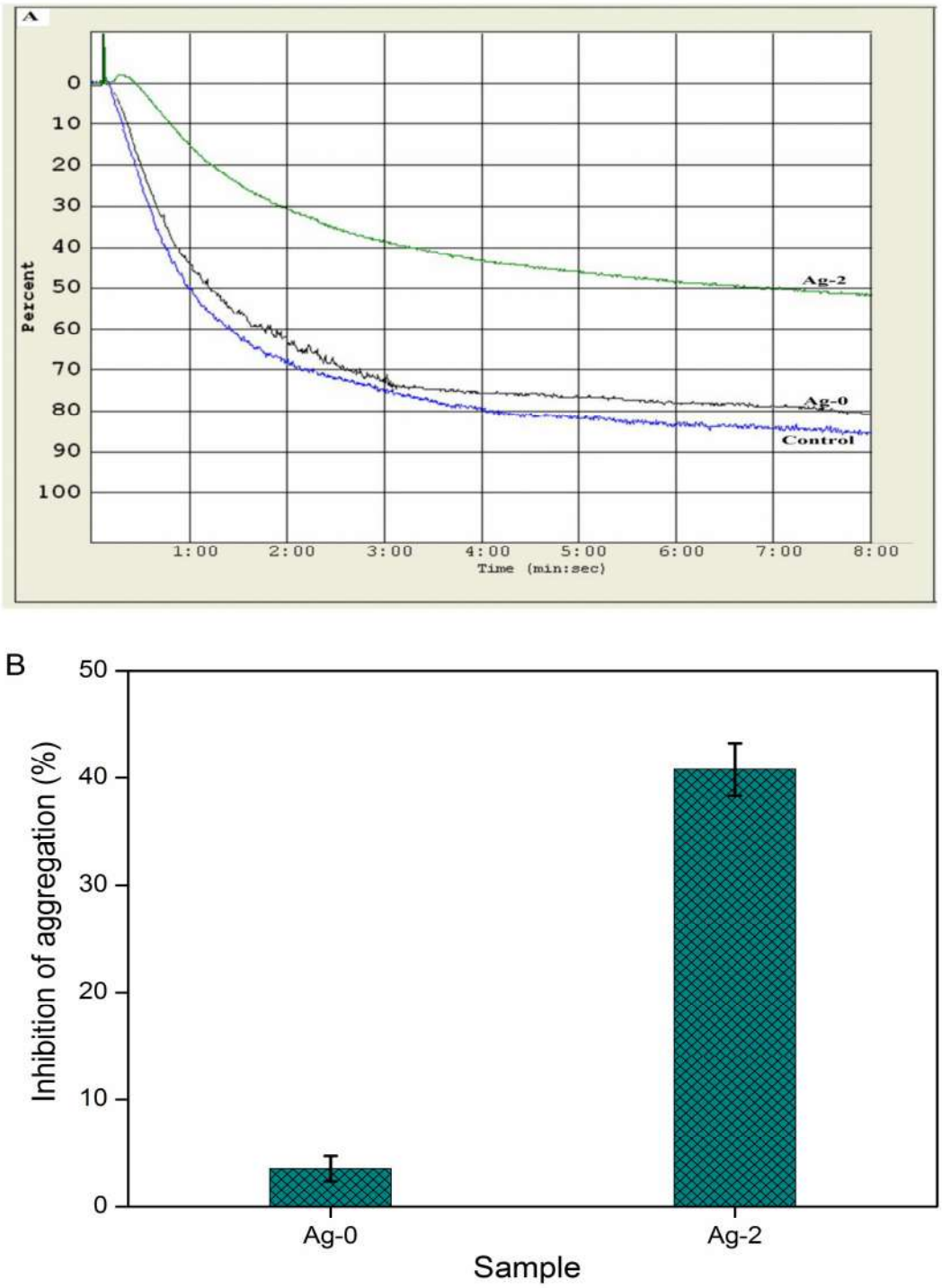


Figure 7.18 *In vitro* blood platelet aggregation behavior after incubation of supernatant of SBF of Ag-0 and Ag-2 BGC samples as well as control (A) the change in % light transmittance with respect to time and (B) the % inhibition of platelet aggregation after 8 min incubation.

### 7.3.10 Antibacterial study

The antibacterial activity of Ag-0 and Ag-2 BCG scaffold samples was performed against *E.coli* bacteria. The test was carried out by disc diffusion method in order to find the zone inhibition by the disc sample in bacterial solution [67][175][190]. It can be clearly seen from the **Figure 7.19** that the sample containing $Ag_2O$ exhibits significant growth inhibition of bacteria and zone formation around the disc in comparison to Ag-0 sample after 24 h of incubation. The zone inhibition of Ag-2 sample was found to be $23 \pm 2$ mm in diameter. The absence of bacteria around the disc sample might be due to the release of $Ag^+$ ions from the sample [64] [67][172,174][191]. It was reported earlier that the release of silver ions from the glass is due to diffusion-controlled mechanism. Moreover, previous studies have also demonstrated that the introduction of $Ag_2O$ into bioactive glass systems via sol-gel route has diminished the risk of bactericidal migration. This was due to the leaching of $Ag^+$ ions from the glass and it elicits rapid antimicrobial activity while preserving its bioactivity [64] [172–174]. In the present investigation, the concentration of $Ag_2O$ in the BG system was competent enough for bacterial migration of *E.coli*. Thus, the results suggest that the prepared scaffold sample demonstrated antimicrobial activity.

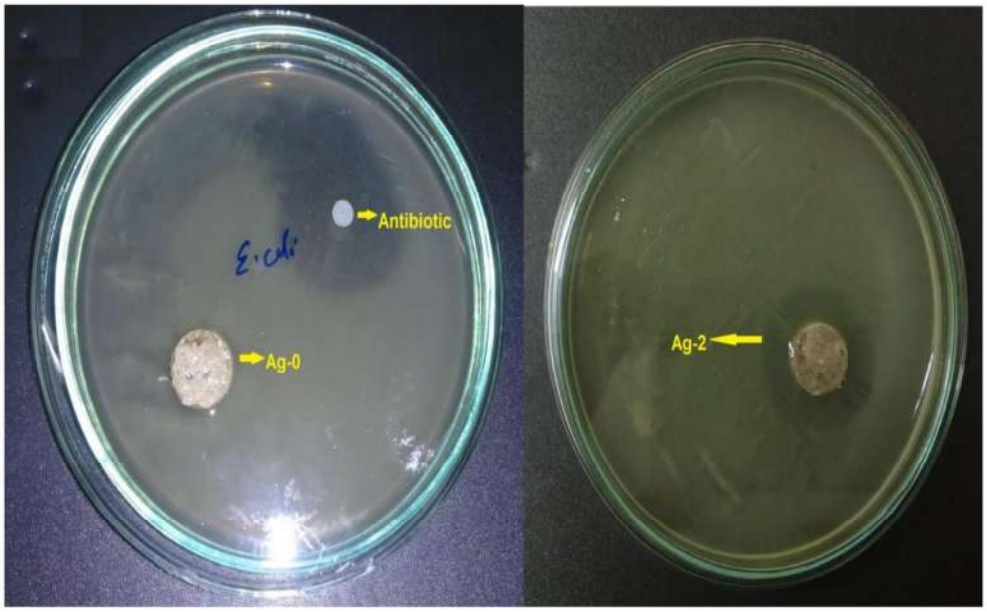


Figure 7.19 Antibacterial effect of Ag-0 and Ag-2 bioactive glass-ceramic scaffold samples against *E.Coli* bacteria

### 7.3.11 In vivo radiograph

X-ray radiographic imaging is a primary and reliable diagnostic technique to examine the pre- and post-surgery status of bone fractures of the patients. The Ag-2 bioactive glass-ceramic scaffold has been implanted in the rat femur bone as shown in photographic images (**Figure 7.20**). After implantation, the X-ray radiographic images were taken at 15 and 30 day as shown in **Figure 7.21**. It can be clearly differentiated from between the sample and the bone radiographic images. After 15 days of implantation, the image showed some gap around the sample while after 30 days of implantation maximum healing had taken place. Therefore, it indicated that as the time of implantation increased the healing of the bone was taking place at the surgery site. This might be due to the enhanced bioactivity of the sample towards the bone healing. It was in good support from the *in vitro* results of XRD (**Figure 7.10 C**) and cell attachment and growth (**Figure 7.15**) on the Ag-2 BGC sample. This suggests that the

sample has encouraged the osteoblast and osteoconduction of bone cells *in vivo* and promoted new bone formation.

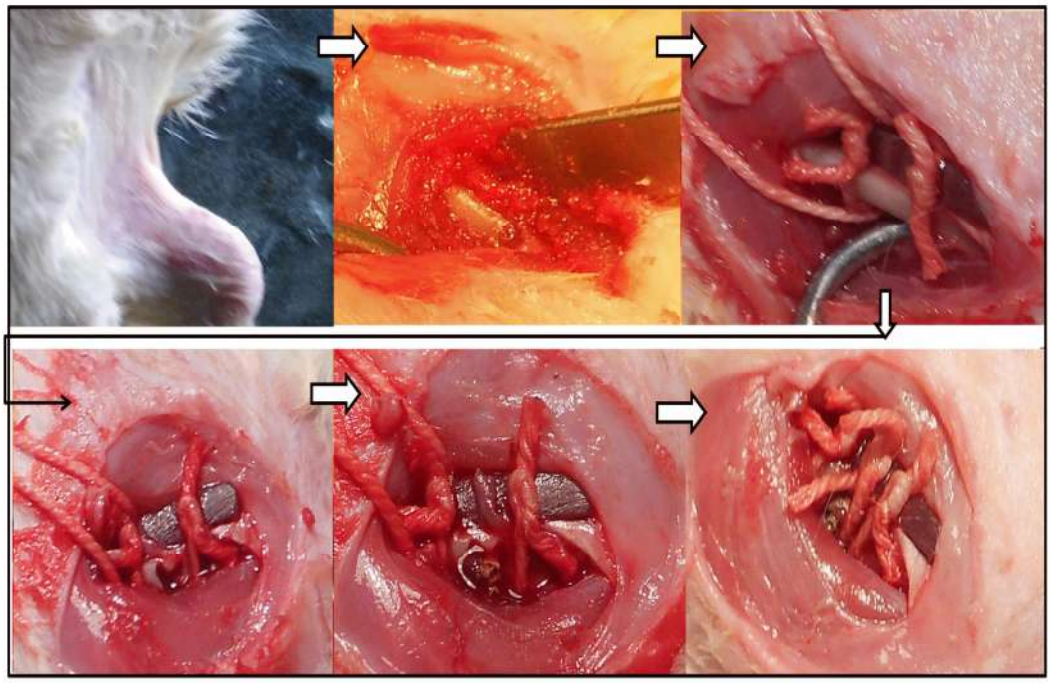

Figure 7.20 Photographic images during implantation of Ag-2 scaffold sample in rat femur bone

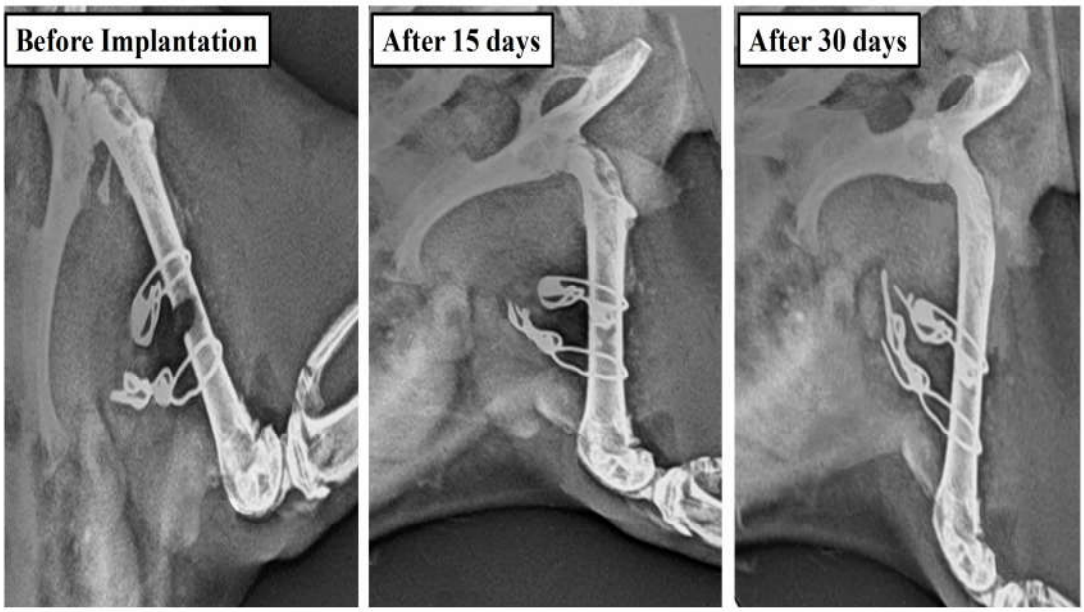


Figure 7.21 X-ray radiographic images before and after implantation for 15 and 30 days of Ag-2 scaffold sample in rat femur bone.

## 7.4 Conclusions

It can be concluded for the results that the bioactive glasses has been successfully prepared by sol gel route with an introduction of $Ag_2O$. The particle size and distribution was found to increase with an increase in Ag content in the bioactive glass samples. All the sintered samples have exhibited the sodium calcium silicate phase while Ag-1 and Ag-2 samples revealed an additional phase of metallic Ag which indicated that the metallic silver was successfully embedded in the glassy matrix as confirmed by XRD and SEM-EDS techniques. During substitution of $Ag_2O$ in the bioactive glass, the Ag was found to present in both the forms as in metallic and ionic states. Further, the porous scaffold was fabricated successfully using sucrose as pore forming agent. The scaffolds have shown good porosity of 68.33 to 57.45% for Ag-0 and Ag-2 samples, respectively and the pores size was found in range of 140 – 700 μm. The compressive strength of the scaffold was found to increase from 2.4 to 18.3 MPa with increasing concentration of $Ag_2O$ in the BG. The *in vitro* bioactivity in SBF demonstrated the formation of HCA layer on the surface of the samples as confirmed by FTIR spectrometry, SEM, XRD and pH behavior. Moreover the HCA layer was more prominent in Ag contained samples. The *in vitro* cell culture studies like cell viability, cytotoxicity and proliferation demonstrated that the scaffold samples were tolerant to the human osteosarcoma U2-OS cell lines and thus the substitution of Ag2O did not cause for cells cytotoxicity and allowed the cell growth. Further, the cells were significantly attached and grown on the surface and porous area as well as pore walls of the Ag-2 BGC sample. The elemental mapping on the Ag-2 scaffold had shown the presence of Ag and its distribution in the sample even after culture for 5 days. All the samples demonstrated good human blood compatibility with RBC and WBC while Ag-2 BGC sample diminished the blood platelet coagulation as compared to Ag-0 BGC

sample. Moreover, the Ag-2 scaffold sample exhibited good antibacterial activity against *E.coli* bacteria which could be due to the release of $Ag^{+}$ ions from the sample. The *in vivo* X-ray radiographic results of Ag-2 scaffold had exhibited the bone healing after 30 days of implantation in rat femur bone. The Ag-contained bioactive glass-ceramic scaffold had demonstrated the multifunctional properties as described above. Therefore, in view of all respects, the prepared scaffold can be used as an implant for bone tissue engineering.

.